In-Cell Chemical Crosslinking Identifies Hotspots for SQSTM-1/p62-IκBα Interaction That Underscore a Critical Role of p62 in Limiting NF-κB Activation Through IκBα Stabilization

Authors

Yi Liu, Michael J. Trnka, Liang He, A. L. Burlingame, and Maria Almira Correia

Correspondence

almira.correia@ucsf.edu

In Brief

The transcriptional activator NF-κB inhibitor, IκBα is proteolytically unstable when uncomplexed. How newly synthesized IκBα escapes degradation to terminate nuclear NF-κB activation is unknown. In-cell chemical crosslinking and proximity labeling MS analyses uncovered a novel association of p62 with IκBα *via* well-defined structural hotspots, which impairs its interaction with 26S/20S proteasome, extends its life-span and enables its termination of NF-κB activation. Mice carrying liver-specific genetic deletion of p62-IκBα hotspot exhibit enhanced liver inflammation upon aging, validating this novel p62 role.

Graphical Abstract

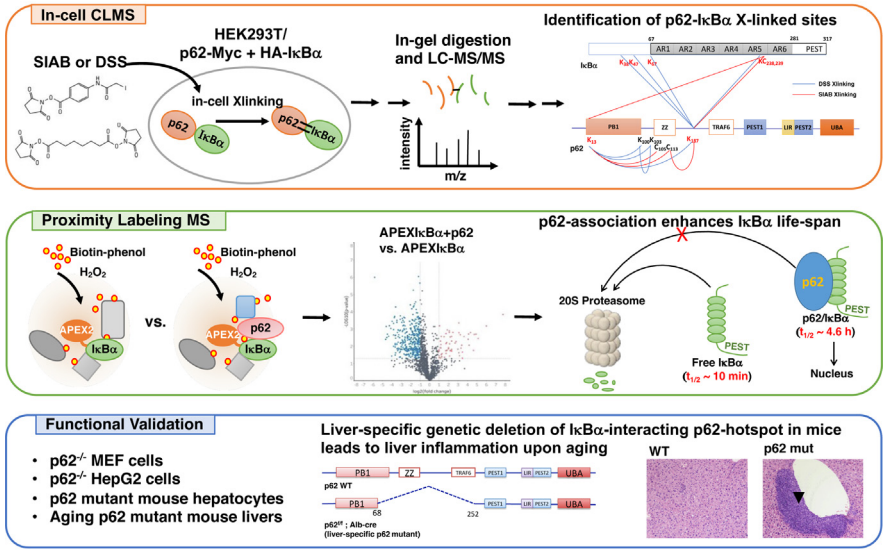

Highlights

- p62 binds to and stabilizes IκBα by preventing its proteolytic degradation.
- In-cell chemical crosslinking/LC-MS/MS identified the inter-crosslinked sites.
- Hotspots of p62-IκBα association are defined.
- APEX proximity labeling revealed p62 impaired IκBα-interaction with proteasome.
- p62 chaperones newly synthesized IκBα to terminate NF-κB activation.

2023, Mol Cell Proteomics *22*(*2*), 100495

https://doi.org/10.1016/j.mcpro.2023.100495

In-Cell Chemical Crosslinking Identifies Hotspots for SQSTM-1/p62-IκBα Interaction That Underscore a Critical Role of p62 in Limiting NF-κB Activation Through IκBα Stabilization

Yi Liu[1], Michael J. Trnka[2], Liang He[1], A. L. Burlingame[2], and Maria Almira Correia[1,2,3,4,*]

We have previously documented that in liver cells, the multifunctional protein scaffold p62/SQSTM1 is closely associated with IκBα, an inhibitor of the transcriptional activator NF-κB. Such an intimate p62-IκBα association we now document leads to a marked 18-fold proteolytic IκBα-stabilization, enabling its nuclear entry and termination of the NF-κB–activation cycle. In $p62^{-/-}$-cells, such termination is abrogated resulting in the nuclear persistence and prolonged activation of NF-κB following inflammatory stimuli. Utilizing various approaches both classic (structural deletion, site-directed mutagenesis) as well as novel (in-cell chemical crosslinking), coupled with proteomic analyses, we have defined the precise structural hotspots of p62-IκBα association. Accordingly, we have identified such IκBα hotspots to reside around N-terminal (K38, K47, and K67) and C-terminal (K238/C239) residues in its fifth ankyrin repeat domain. These sites interact with two hotspots in p62: One in its PB-1 subdomain around K13, and the other comprised of a positively charged patch ($R_{183}/R_{186}/K_{187}/K_{189}$) between its ZZ- and TB-subdomains. APEX proximity analyses upon IκBα-cotransfection of cells with and without p62 have enabled the characterization of the p62 influence on IκBα–protein-protein interactions. Interestingly, consistent with p62's capacity to proteolytically stabilize IκBα, its presence greatly impaired IκBα′s interactions with various 20S/26S proteasomal subunits. Furthermore, consistent with p62 interaction with IκBα on an interface opposite to that of its NF-κB–interacting interface, p62 failed to significantly affect IκBα–NF-κB interactions. These collective findings together with the known dynamic p62 nucleocytoplasmic shuttling leads us to speculate that it may be involved in "piggy-back" nuclear transport of IκBα following its NF-κB–elicited transcriptional activation and *de novo* synthesis, required for termination of the NF-κB–activation cycle. Consequently, mice carrying a liver-specific deletion of p62-residues 68 to 252 reveal age-dependent–enhanced liver inflammation. Our findings reveal yet another mode of p62-mediated pathophysiologically relevant regulation of NF-κB.

The nuclear factor kappa-light-chain-enhancer of activated B cells (NF-κB) is a major transcriptional factor responsible for the nuclear activation of genes involved in myriad cellular processes, including inflammation, immune response, and cancer. In the liver as in many cells, NF-κB exists largely as a p65/p50 heterodimer that is sequestered in the cytoplasm and kept transcriptionally inactive through its tight binding to specific NF-κB inhibitors (IκBs), which mask its nuclear localization signal (NLS) and DNA-binding domain (1). Of these IκBs, IκBα and IκBβ are the major isoforms in liver cells and cell-lines, each regulated by different extracellular signals and/or cues (2–5). Canonical transcriptional activation of NF-κB–responsive genes triggered by appropriate extracellular signals such as proinflammatory cytokines entails the disruption of IκB-mediated NF-κB tethering *via* IKK-elicited phosphorylation of IκB–N-terminal $Ser_{32/36}$-residues that in turn triggers their ubiquitin (Ub)-dependent 26S proteasomal degradation (6–8). Such IκB destruction unleashes NF-κB, unmasking its NLS and enabling its nuclear translocation and subsequent DNA association and transcriptional activation of NF-κB–responsive genes including those of IκBα (but not IκBβ) (9–12) and p62/SQSTM1 (13–18), as well as immune and inflammatory-response genes. This NF-κB–mediated transcriptional activation of the IκBα gene results in *de novo* IκBα synthesis which upon nuclear reentry, strips off the DNA-bound NF-κB, escorting it out of the nucleus into the cytoplasm, thereby aborting further NF-κB activation and resetting the system to baseline (9, 11, 15, 16, 19). However, unbound

From the [1]Department of Cellular & Molecular Pharmacology, [2]Department of Pharmaceutical Chemistry, [3]Department of Bioengineering and Therapeutic Sciences, and [4]The Liver Center, University of California San Francisco, San Francisco, California, USA
*For correspondence: Maria Almira Correia, almira.correia@ucsf.edu.

https://doi.org/10.1016/j.mcpro.2023.100495

(free) IκBα has an extremely short half-life (20), thus, how newly synthesized IκBα that lacks a *bona fide* canonical NLS escapes from degradation and gains nuclear entry remains unknown.

We have previously reported that in liver cells, the cellular multifunctional protein scaffold p62/SQSTM1 is closely associated with IκBα, coaggregating with it upon Zn-protoporphyrin IX (ZnPP)-elicited protein aggregation (21). Their association, however, is not required for ZnPP-elicited IκBα sequestration into insoluble aggregates resembling hepatic Mallory-Denk bodies, as such ZnPP-elicited IκBα aggregation is unscathed upon p62-KO of mouse embryo fibroblasts (MEFs) as well as primary hepatocytes (21). Herein, we elucidate a novel feature of such an exquisite p62–IκBα intracellular interaction, which by enabling p62 to chaperone the newly synthesized IκBα extends its otherwise extremely short intracellular half-life, and by providing its intrinsic NLS-domain, p62 plausibly facilitates intranuclear IκBα-transport, consequently regulating the IκBα/NF-κB–mediated vicious inflammatory cycle. Accordingly, we document that in contrast to that in corresponding WTs, $p62^{-/-}$-MEF cells as well as CRISPR-Cas9–edited $p62^{-/-}$ HepG2 cells exhibit not only a considerably blunted IκBα-feedback response (restoration) after TNFα or IL-1β stimulation but also show a relatively more pronounced and prolonged nuclear p65-localization. More importantly, by using a novel in-cell chemical crosslinking mass spectrometry (XLMS) approach, we further identify a previously unrecognized p62-domain for IκBα-binding, whose direct interaction results in extending the physiological IκBα half-life ($t_{1/2}$) and thus enabling its efficient termination of NF-κB activation. Accordingly, we document that liver-specific genetic deletion of this p62 IκBα-binding domain in intact mice leads to severe hepatic inflammation upon aging, most likely by destabilizing IκBα and thereby disrupting the normal termination of NF-κB activation elicited upon *de novo* IκBα synthesis. These findings attest to an exquisite role for p62 in the regulation of NF-κB-IκBα–mediated physiological and pathophysiological processes.

EXPERIMENTAL PROCEDURES

p62-Mutant Mice and p62-KO Cell Lines

p62mut Mice—We set out to generate p62 liver-conditional KO mice in C57BL/6N strain (C57BL/6N-Sqstm1$^{tm1a(KOMP)Wtsi}$/Mmucd) with the assistance of UC Davis KOMP Facility starting from frozen embryos carrying Sqstm1/p62 tm1a KO allele. The KOMP Facility generated the tm1c heterozygous mice that were provided to us. We first bred these mice to obtain the homozygous p62 flp/flp tm1c mice that were in turn employed for Alb-Cre deletion to generate the liver-conditional p62 KO mice. For this purpose, Alb-Cre homozygous mice purchased from Jackson Laboratory (strain 003574) were bred with the p62 flp/flp homozygous mice. The resulting pups, all p62 flp/+, Albcre/+ heterozygous, were then bred with the p62 flp/flp homozygous mice with 25% of the resulting pups being p62 flp/flp, Albcre/+, thus carrying specifically in the liver, a copy of Albcre recombinase to delete out the FLPed region in the p62 gene. After obtaining the p62 flp/flp, Albcre/+ conditional KO mice, p62 flp/flp, Albcre/+ mice were bred with p62 flp/flp mice, such that 50% of the pups would be p62 liver-conditional KOs and the other 50% of pups, the WT controls. Immunoblotting (IB) analyses of their hepatic p62 content and RT-PCR analyses followed by sequencing revealed however that instead of the anticipated liver-conditional p62 KO, a structural deletion mutant (p62mut), with the deletion of the region coding for amino acid residues 68 to 252, was obtained. Mice were fed a standard chow diet and maintained under 12-h light/dark cycle. All animal experimental protocols were approved by the UCSF/Institutional Animal Care and Use Committee.

p62 KO MEF Cells—p62 KO MEF cells were generated from p62 KO mice by Prof. M. Komatsu's lab (22) and provided by Prof. Haining Zhu, University of Kentucky.

p62 KO HepG2 Cells—The CRISPR/Cas9 system was used to knockout p62 in HepG2 cell line. The CRISPR guide RNAs were designed using CRISPR Design online tool (23). A sequence targeting exon 3 (TCAGGAGGCGCCCCGCAACA**TGG**) was used. Oligonucleotide containing the CRISPR target sequence was annealed and ligated into Bbs1 linearized pSpCas9(BB)-2A-Puro (PX459) vector (Addgene #48139). HepG2 cells were transfected with PX459-p62 with X-tremeGENE HP transfection reagent (Roche). Twenty-four hours after transfection, cells were exposed to medium containing puromycin and selected for 48 h, after which, cells were recovered with an antibiotic-free medium for 24 h before reseeding into 100-mm dishes at 100 cells/dish. Cells were allowed to grow for 4 to 8 weeks until single cell colonies appeared. Single cell colonies were then picked and expanded for screening using Western IB analyses as guidelines.

Cell Culture and Transfections

p62mut mice and age-matched WT litter-mates (8- to 12-week old) bred in our lab were used for primary hepatocyte preparation. Hepatocytes were isolated by *in situ* collagenase perfusion and purified by Percoll-gradient centrifugation by the UCSF Liver Center Cell Biology Core, as described previously (24). Fresh primary mouse hepatocytes were cultured on Type I collagen-coated 60 mm Permanox plates (Thermo Fisher Scientific) in William's E Medium (Gibco) supplemented with 2 mM L-glutamine, insulin-transferrin-selenium (Gibco), 0.1% bovine albumin Fraction V (Gibco), Penicillin-Streptomycin (Gibco), and 0.1 μM dexamethasone. Cells were allowed to attach overnight and then overlaid with Matrigel by replacing with fresh media containing Matrigel (0.25 mg/ml; Corning). From the second day after plating, the medium was replaced daily, and cells were further cultured for 4 to 5 days with daily light microscopic examination for any signs of cell death and/or cytotoxicity. On day 5, some cells were treated with IL-1β (20 ng/ml) for 15 min, and cells were then harvested at indicated timepoints using a cell scraper.

HepG2 cells were cultured in minimal Eagle's medium containing 10% v/v fetal bovine serum (FBS) and supplemented with nonessential amino acids and 1 mM sodium pyruvate. HEK293T and MEF cells were cultured in Dulbecco's Modified Eagle high glucose medium containing 10% v/v FBS. For transfection experiments, cells were seeded on 6-well plates; when cells were 60% confluent, each cell well was transfected with 3 μg of plasmid DNA complexed with TurboFect transfection reagent (Thermo Fisher Scientific) for HEK293T cells and X-tremeGENE HP transfection reagent (Roche) for HepG2 cells, according to the manufacturers' instructions. At 40 to 72 h after transfection, cells were either treated as indicated or directly harvested for assays. For NF-κB activation assays, HepG2 cells or MEF cells were first rested in FBS-free medium for 4 h, then treated with

TNFα (20 ng/ml) or IL-1β (20 ng/ml) for indicated times, after which cells were harvested using a cell scraper.

Plasmids

pSpCas9(BB)-2A-Puro (PX459) was a gift from Dr Feng Zhang (Addgene plasmid # 48139; http://n2t.net/addgene:48139; RRID: Addgene_48139) (25). pCMV-3HA-IκBα and pCMV-3HA-IκBα-S_{32}A/S_{36}A were gifts from Dr Warner Greene (plasmids #21985, #24143; Addgene). pLX304-Flag-APEX2-NES were gifts from Dr Alice Ting (Addgene plasmid # 92158; http://n2t.net/addgene:92158; RRID: Addgene_92158) (26). C1-Emerald was a gift from Dr Michael Davidson (Addgene plasmid #54734). pcDNA6 and pcDNA3 vectors were from Invitrogen. C1-Emerald-IκBα, pcDNA6-p62-myc were constructed in house previously (21). Various IκBα and p62 mutants were constructed for this study. Truncation mutations were constructed by PCR cloning, or DNA fragment gene synthesis, or homologous recombination-based NEBuilder HiFi DNA Assembly kit (NEB). Site-directed mutagenesis was carried out using a QuikChange Site-Directed Mutagenesis Kit (Agilent). The primers, templates, vectors, and restriction enzymes used are summarized below:

Plasmid	Template	PCR primers (restriction sites underlined)	Vector	Restriction enzymes
pcDNA6-p62-myc **ΔZZ** (128–163)	N/A	N/A, synthesized p62 DNA fragment with 382–489 deleted	pcDNA6-myc/His	*XhoI*/*HindIII*
pcDNA6-p62-myc **ΔTB** (225–251)	N/A	N/A, synthesized p62 DNA fragment with 672–753 deleted	pcDNA6-myc/His	*XhoI*/*HindIII*
pcDNA6-p62-myc **N127**	pTOPO-p62	AAGCTT**ATG**GCGTCGCTCACCG CTCGAGGATCACATTGGGGTGCACC	pcDNA6-myc/His	*XhoI*/*HindIII*
pcDNA6-p62-myc **N224**	pTOPO-p62	AAGCTT**ATG**GCGTCGCTCACCG CTCGAGTGATTCTGCCGTGGGGCC	pcDNA6-myc/His	*XhoI*/*HindIII*
pcDNA6-p62-myc **N265**	pTOPO-p62	AAGCTT**ATG**GCGTCGCTCACCG CTCGAGTCTTTTCCCTCCGTGCTCCAC	pcDNA6-myc/His	*XhoI*/*HindIII*
pcDNA6-p62-myc **N320**	pTOPO-p62	AAGCTT**ATG**GCGTCGCTCACCG CTCGAGCCCCTCGGACTCCAAGGCG	pcDNA6-myc/His	*XhoI*/*HindIII*
pcDNA6-p62-myc **N385**	pTOPO-p62	AAGCTT**ATG**GCGTCGCTCACCG CTCGAGATGTGGGTACAAGGCAGCTTCC	pcDNA6-myc/His	*XhoI*/*HindIII*
pcDNA6-p62-myc **C225**	pTOPO-p62	AAGCTT**ATG**GCTTCTGGTCCATCGGAGG CTCGAGCAACGGCGGGGGATGC	pcDNA6-myc/His	*XhoI*/*HindIII*
pcDNA6-p62-myc **C164**	pTOPO-p62	AAGCTT**ATG**ACCAAGCTCGCATTCCCC CTCGAGCAACGGCGGGGGATGC	pcDNA6-myc/His	*XhoI*/*HindIII*
pcDNA6-p62-myc **C104**	pTOPO-p62	AAGCTT**ATG**GAGTGCCGGCGGGACCACC CTCGAGCAACGGCGGGGGATGC	pcDNA6-myc/His	*XhoI*/*HindIII*
pcDNA6-p62-myc **$LL_{10}AA$**	pTOPO-p62	CTCACCGTGAAGGCCTACGCTGCAGGC AAGGAGGACGCGGCG CGCCGCGTCCTCCTTGCCTGCAGCGTA GGCCTTCACGGTGAG	pcDNA6-myc/His	*XhoI*/*HindIII*
pcDNA6-p62-myc **$K_{13}A$**	pTOPO-p62	CTACCTTCTGGGCGCGGAGGACGCGGCGC GCGCCGCGTCCTCCGCGCCCAGAAGGTAG	pcDNA6-myc/His	*XhoI*/*HindIII*
pcDNA6-p62-myc **$DE_{14}AA$**	pTOPO-p62	CTACCTTCTGGGCAAGGCAGCTGCGG CGCGCGAGATTCGC GCGAATCTCGCGCGCCGCAGCTGCC TTGCCCAGAAGGTAG	pcDNA6-myc/His	*XhoI*/*HindIII*
pcDNA6-p62-myc **$H_{190}A$**	pTOPO-p62	GGCTTCGGAAGCTGAAAGCTGGACACTTT GGCTGGC GCCAGCCAAAGTGTCCAGCTTTCAGCTT CCGAAGCC	pcDNA6-myc/His	*XhoI*/*HindIII*
pcDNA6-p62-myc **$WL_{184}AA$**	pTOPO-p62	GCTTCTCGCACAGCCGCGCGGCCCGG AAGGTGAAACAC GTGTTTCACCTTCCGGGCCGCGCGGCTGTG CGAGAAGC	pcDNA6-myc/His	*XhoI*/*HindIII*
pcDNA6-p62-myc **$KK_{187}AA$**	pTOPO-p62	GCCGCTGGCTCCGGGCGGTGGCACA CGGACACTTCG CGAAGTGTCCGTGTGCCACCGCCCGG AGCCAGCGGC	pcDNA6-myc/His	*XhoI*/*HindIII*
pcDNA6-p62-myc **RRKK-A ($R_{183}R_{186}K_{187}K_{189}AAAA$):**	pTOPO-p62	GGGCTTCTCGCACAGCGCCTGGCT CGCGGCGGTGGCACACGGACACTTCGGG CCCGAAGTGTCCGTGTGCCACCGCCG CGAGCCAGGCGCTGTGCGAGAAGCCC	pcDNA6-myc/His	*XhoI*/*HindIII*

—*Continued*

Plasmid	Template	PCR primers (restriction sites underlined)	Vector	Restriction enzymes
pCMV4-3HA-IκBα **44–317**	pCMV4-3HA-IκBα	AAGCTTACCCAGATGGTCAAGGAGC CCCGGGATCCTCTAGATCATAACG	pCMV4-3HA-IκBα	*HindIII/SmaI*
pCMV4-3HA-IκBα **67–317**	pCMV4-3HA-IκBα	AAGCTTACCAAGCAGCAGCTCACCG CCCGGGATCCTCTAGATCATAACG	pCMV4-3HA-IκBα	*HindIII/SmaI*
pCMV4-3HA-IκBα **104–317**	pCMV4-3HA-IκBα	GGAAGTTGAGAGCGTAATCTGGAACG TCATATGG AGATTACGCTCTCAACTTCCAGAA CAACCTGC	N/A HiFi DNA Assembly	*N/A*
pCMV4-3HA-IκBα **1–206**	pCMV4-3HA-IκBα	AAGCTTACC**ATG**TTCCAGGCGGCCGAG CCCGGGTCAACCCAAGGACACC AAAAGCTCC	pCMV4-3HA-IκBα	*HindIII/SmaI*
pCMV4-3HA-IκBα **1–287**	pCMV4-3HA-IκBα	AAGCTTACC**ATG**TTCCAGGCGGCCGAG CCCGGGTCACTCCTCATCCTCACTCT CTGGCAGC	pCMV4-3HA-IκBα	*HindIII/SmaI*
pCMV4-3HA-IκBα **104–209**	pCMV4-3HA-IκBα **104–317**	CTCTAGATCAGACATCAGCACCCAA GGACAC TGCTGATGTCTGATCTAGAGGATCCC GGGTGGC	N/A Hifi DNA Assembly	*N/A*
pCMV4-3HA-IκBα **104–199**	pCMV4-3HA-IκBα **104–317**	CTCTAGATCACACGATGCCCAGGTA GCCATG GGGCATCGTGTGATCTAGAGGATCCC GGGTGGC	N/A Hifi DNA Assembly	*N/A*
pCMV4-APEX2-IκBα	pLX304-Flag-APEX2-NES	TCGAATTCAGATCTGGTACGCCACCATGG ACTACAAGGATG CCGCCTGGAACATGGTAAGCTTGCCT GATCCGCTT GTGCTACCTGACCCGGCATCAGCAAA CCCAAGCTC	pCMV4-3HA-IκBα Hifi DNA Assembly	*KpnI/HindIII to cut out HA and linearize vector*

The nucleotides in bold indicate the start codon of the primer sequence.

Cell Fractionation

For whole cell lysate preparation, cells were harvested in cell lysis buffer (CSL buffer, Cell Signaling Technology) containing 20 mM Tris–HCl (pH 7.5), 150 mM NaCl, 1 mM EDTA, 1 mM EGTA, 1% Triton, 2.5 mM sodium pyrophosphate, 1 mM β-glycerophosphate, 1 mM Na_3VO_4, leupeptin (1 μg/ml) and supplemented with 10% glycerol and a protease/phosphatase inhibitor cocktail (Pierce). Cell lysates were sonicated for 10 s and then cleared by centrifugation at 4 °C in a tabletop centrifuge at 14,000*g* for 10 min. Nuclear and cytoplasmic extracts were prepared using NE-PER Nuclear and Cytoplasmic Extraction Kit (Thermo Fisher Scientific). Briefly, cells were harvested in PBS supplemented with a protease/phosphatase inhibitor cocktail and pelleted at 400*g* for 5 min at 4 °C. Cell pellet collected from one 60 mm Petri dish was first resuspended in CER I buffer (400 μl) and incubated on ice for 10 min. Then, CER II (22 μl) was added and the mixture vortexed, followed by incubation on ice for 1 min. The tubes were then centrifuged at 14,000*g* for 5 min at 4 °C. The supernatants were then transferred into a new tube as cytoplasmic extracts. The tubes containing the pellet were then washed briefly with PBS and centrifuged briefly, and the residual supernatants were discarded. The pellets were then resuspended in ice-cold NER buffer (150 μl) and sonicated for 5 s to disrupt the pellets. The tubes were centrifuged at 14,000*g* for 5 min at 4 °C, and the supernatants were recovered as the nuclear extracts. Mitochondrial extracts were prepared using Mitochondria Isolation Kit for Cultured Cells (Thermo Fisher Scientific) with some modifications. Briefly, cells from three 60 mm Petri dishes were harvested in PBS supplemented with a protease/phosphatase inhibitor cocktail and combined and pelleted at 400*g* for 5 min at 4 °C. The pellets were then resuspended in Reagent A (600 μl) and incubated on ice for 2 min. Resuspended cells were then disrupted using a micro-tip homogenizer (Omni-Inc) for 40 s, twice. Reagent C (600 μl) was then added and mixed by inverting the tube several times. The tubes were then centrifuged at 700*g* for 10 min at 4 °C. Nucleus and unbroken cells were pelleted at this step. The supernatants containing the cytoplasmic fraction were transferred to a new tube and then centrifuged at 12,000*g* for 20 min at 4 °C. The supernatants (cytosolic fractions) were recovered and saved. The pellets were washed in Reagent C (200 μl) and then centrifuged at 12,000*g* for 5 min at 4 °C. The supernatants were discarded and pellets were saved as the isolated mitochondria. Isolated mitochondria were then lysed in RIPA buffer (Cell Signaling Technology) supplemented with 0.1% SDS, 10% glycerol, and a protease/phosphatase inhibitor cocktail with sonication. The pellet containing the nuclei and unbroken cells was first resuspended in Triton containing cell lysis buffer with gentle pipetting to lyse unbroken cells but keeping the nuclei intact. The nuclei were then pelleted by centrifugation at 12,000*g* for 5 min at 4 °C, and the pellet was extracted using RIPA buffer with sonication, the resulting lysate was used as the nuclear extract.

Western IB Analyses

For Western IB analyses, extracts from various cell fractions were prepared as described above. Protein concentrations were determined by the bicinchoninic acid assay and equal amounts of proteins were separated on 4 to 15% Tris-Glycine eXtended (TGX)

polyacrylamide gels. Proteins were transferred onto 0.2 μm nitrocellulose membranes (Bio-Rad) for IB analyses.

The following primary antibodies were used: c-Myc (9B11, Cell Signaling Technology), HA (C29F4, Cell Signaling Technology), IκBα (C-terminus, 44D4, Cell Signaling Technology), Phospho-IκBα (Ser_{32}) (14D4, Cell Signaling Technology), p62 (2C11, Abnova), NF-κB p65 (D14E12, Cell Signaling Technology), Phospho-NF-κB p65 (93H1, Cell Signaling Technology), β-Actin (Sigma), Histone H3 (Abcam), COX IV (3E11, Cell Signaling Technology).

Co-Immunoprecipitation Analyses

Whole-cell extracts were prepared as described above. Cell lysates (1 mg) were then incubated with EZview Red Anti-HA Affinity Gel (30 μl; MilliporeSigma) or ChromoTek Myc-Trap Agarose (30 μl; Proteintech) at 4 °C overnight and then eluted by heating at 70 °C for 10 min in 2× SDS-loading buffer. Eluates were subjected to IB analyses as described above.

In-Cell Chemical Crosslinking and Crosslinked Protein Capture for LC-MS/MS

For each crosslinking, ten 100 mm Petri dishes of cultured HEK293T cells were cotransfected with pCMV4-3HA-IκBα and pcDNA6-p62-myc at a 1:1 ratio for 48 h. For disuccinimidyl suberate (DSS)-crosslinking, cells were treated with 10 mM NEM for 5 min right before harvesting. Cells were then washed three times using ice-cold PBS and collected by a cell scraper in PBS. After that, DSS (0.05 mM) or SIAB [(succinimidyl (4-iodoacetyl)aminobenzoate); 0.05 mM] was added directly to the cell suspension and mixed gently by inversion and incubated on a rocker platform for 20 min in the dark. Tris buffer pH 7.4 was then added to a final concentration of 20 mM to quench the crosslinking reaction. Cells were pelleted and then lysed in RIPA buffer supplemented with 10 mM NEM (or 10 mM iodoacetamide for SIAB-crosslinked cells) with sonication and cleared by centrifugation. The supernatant was then incubated with Myc-Trap (500 μl) overnight at 4 °C to pull-down Myc-tagged p62 and HA-IκBα–crosslinked Myc-tagged p62. Beads were then washed three times using RIPA buffer and then eluted by heating at 70 °C for 10 min in 2× SDS-loading buffer containing 4% SDS. Eluates were then diluted 20 times using CSL buffer and incubated with HA-agarose (100 μl) overnight at 4 °C. Subsequently, beads were collected by centrifugation at 3000*g* for 30 s and then washed three times with RIPA buffer and then eluted by heating at 70 °C for 10 min in 2× SDS-loading buffer. This tandem IP resulted in an enrichment of p62-Myc– and HA-IκBα–crosslinked species. Eluates were then split into 4 to 5 gel lanes and subjected to SDS-PAGE and stained with Coomassie Blue to visualize the bands for subsequent in-gel digestion.

IR Fluorescence Detection of DSS- or SIAB-Crosslinked p62-IκBα Species

Western IB analysis of the crosslinked p62–IκBα complexes was first carried out with a two-color system using IRDye 680RD goat anti-mouse IgG for labeling p62-Myc and IRDye 800CW goat anti-rabbit IgG for HA-IκBα, which were then detected by IR fluorescence detection with an Odyssey Fc Imaging System (LI-COR Biosciences).

APEX Reaction and Biotinylated Protein Capture

APEX biotinylation was carried out as described by Hung *et al.* (26). Briefly, HEK293T cells grown in 60-mm Petri dishes were transfected with N-terminal pCMV4-APEX2-IκBα with or without pcDNA6-p62-Myc cotransfection. mEmerald (GFP)-tagged IκBα (GFP-IκBα) cotransfected with pcDNA6-p62-Myc were used as a negative control. Forty-eight hours after transfection, cells were treated with 500 μM biotin-phenol for 30 min. H_2O_2 was then added to a final concentration of 1 mM for 1 min to initiate the catalytic biotinylation labeling. The labeling reaction was then stopped by quickly exchanging the media with PBS containing 500 mM sodium ascorbate and 5 mM sodium azide. Cells were further washed two times with the antioxidant-containing PBS buffer and then lysed in RIPA buffer. Cell lysates were cleared by centrifugation at 14,000*g*, and the supernatants were screened by Western IB analyses with streptavidin (SA)-HRP to determine the extent of the biotinylation, with subsequent SA pull-downs to enrich the biotinylated proteins. For SA pull-downs, Pierce Streptavidin Magnetic Beads (75 μl; Thermo Fisher Scientific) were added to the lysates and the mixture incubated at 4 °C overnight on a rotator. Beads were then washed twice with RIPA buffer, once with 1 M KCl, once with 2 M urea in 20 mM Tris base, twice with RIPA buffer, and lastly twice with 100 mM ammonium bicarbonate (ABC) before proceeding with the on-bead digestion.

Mass Spectrometric Analyses

For in-gel digestion of in-cell crosslinked samples, the indicated gel bands from 4 or 5 replicate lanes were pooled and processed using a standard in-gel digestion procedure (27, 28). Briefly, each gel piece was excised into 1 mm × 1 mm pieces, reduced and alkylated, and then digested overnight with 300 ng of Trypsin/Lys-C Mix (Promega). For on-bead digestion following SA pull-down, beads were first resuspended in 6 M urea, 100 mM ABC buffer, and then reduced by addition of 10 mM (final) DTT and incubation at 37 °C for 30 min. The samples were then alkylated with 15 mM (final) iodoacetamide (NEM was used for DSS-crosslinked samples) at room temperature in the dark for 30 min. Trypsin/Lys-C Mix (100 ng) was then added, and the mixture was incubated for 4 h at 37 °C. Samples were diluted 1:6 (v:v) with 100 mM ABC to reduce the urea concentration to 1 M and then further incubated at 37 °C overnight. The resulting peptide mixture was desalted using C18-Zip tips (EMD Millipore), speed-vacuumed to dryness, and suspended in 0.1% formic acid for injection into a Q-Exactive Plus (for APEX experiments), an LTQ-Orbitrap Velos (for SIAB cross-linking), or an Orbitrap Fusion Lumos (for DSS cross-linking) mass spectrometer (Thermo Fisher Scientific) coupled through an EASY-Spray nano ion source (Thermo) to a nano-Acquity UPLC (Waters) running an EASY-Spray column (75 μm × 15 cm column packed with 3 μm, 100 Å PepMap C18 resin; Thermo). The mobile phases were as follows: solvent A, water/0.1% formic acid; solvent B, acetonitrile/0.1% formic acid.

For APEX analyses, the samples were loaded at 600 nl/min of 2% B, followed by elution at 400 nl/min with a gradient to 23% B over 103 min and then a second gradient to 40% B in 11 min followed by washing at 75% B and reequilibration. Total run time was 150 min. Precursor ions were acquired from 350 to 1500 m/z (70k resolving power, 3e6 automatic gain control (AGC), 100 ms max injection time), the top ten doubly charged or higher precursor ions were selected with a 4 m/z window, dissociated with 25% normalized collision energy (NCE) higher-energy collisional dissociation (HCD), and measured at 17.5k resolving power (5e4 AGC, 120 ms max injection time). A 15 s dynamic exclusion window was used.

DSS-crosslinked samples were loaded at 600 nl/min at 2% B and then eluted with a 400 nl/min gradient from 3 to 27% B over 92 min. The column was then washed at 75% B and reequilibrated back to 2%. The total run time was 120 min. Precursor ions were acquired from 375 to 1500 m/z in the Orbitrap (120k resolving power, 4e5 AGC, 50 ms max injection time). The top nine precursors with charges 3 to 8+ and intensity greater than 50,000 were isolated in the quadrupole (1.6 m/z selection window) and sequentially dissociated by HCD with stepped 25, 30, 35% NCE, and electron transfer/HCD (25 ms ETD reaction time with 10% supplemental HCD activation). Product ions were acquired in the Orbitrap (30k resolving power, 1e5 AGC, 150 ms

max injection time). Thirty second dynamic exclusion and the peptide monoisotopic ion precursor selection option were enabled.

SIAB-crosslinked samples were loaded at 600 nl/min 3% B and then eluted at 300 nl/min with a gradient from 3 to 28% B over 90 min. The column was then washed at 75% B and reequilibrated with a total run time of 125 min. Precursor ions were acquired in the Orbitrap from 300 to 1800 m/z (30k resolving power, 2e6 AGC, 100 ms max injection time). The top six, 3+ and higher precursors with intensity greater than 4000 were isolated in the quadrupole (4 m/z isolation window) and dissociated by HCD (30% NCE). Product ions were measured in the Orbitrap (7.5k resolving power, 9e4 AGC, max injection time 500 ms).

For APEX analyses, peak lists were extracted using PAVA, an in-house software developed by the UCSF Mass Spectrometry Facility. Peak lists were searched against the SwissProt human database (SwissProt.2019.4.8; 20,418 entries searched) using Protein Prospector (version 5.19.1; http://prospector.ucsf.edu/prospector/mshome.htm) (29). A fully randomized decoy database (an additional 20,418 entries) was used to estimate false discovery rates (FDRs) (30). Protein Prospector search parameters were as follows: tolerance for precursor and product ions were 20 ppm and 30 ppm, respectively; a maximum of one missed cleavage of trypsin was allowed; carbamidomethylation of Cys was set as a fixed modification; variable modifications were set to N-terminal Met loss and/or acetylation, Met oxidation, peptide N-terminal Gln to pyroGly conversion; the maximum number of variable modifications was 2. Reporting thresholds were as follows: minimum score of protein: 22.0; minimum score of peptide: 15.0; maximum E value of protein: 0.01; maximum E value of peptide: 0.05. These score thresholds resulted in a <1% FDR at the peptide level and 5% FDR at the protein level.

For crosslinking analyses of the double affinity–purified IκBα, p62 pulldowns, peak lists corresponding to the excised gel bands were initially searched to identify the most abundant proteins in the sample. As expected, p62 and IκBα were detected at an order of magnitude greater abundance measured by normalized spectral abundance factor (NSAF) (31) than other endogenous (*i.e.*, not obviously artifactual) human proteins (supplemental Table S4). A restricted database consisting of all proteins detected with more than one unique peptide and NSAF values within two orders of magnitude of the most abundant protein was used in the crosslinking search (DSS: 28 sequences total, SIAB: 25 sequences. supplemental Table S4 protein IDs: purple accession numbers). For each sequence in the target database, one decoy sequence was generated with a length 10× longer than the reference sequence. For each position, a random amino acid was chosen, weighted by the proteome-wide frequency of amino-acid distributions. Randomized and 10× longer decoy database of the target sequences were used for FDR control and scoring model training. Peak lists were searched with Protein Prospector v6.4.23 with Trypsin specificity and two missed cleavages. Precursor and product ion tolerance were 6 and 12 ppm respectively. DSS or SIAB crosslinking was specified with 5000 intermediate hits saved, and the rank of the best peptide was restricted to 1. For DSS experiments, NEM modification of Cys was used as a constant modification. For SIAB experiments, no constant modification was specified, and carbamidomethylation of Cys was included as a variable modification. For both experiments, variable modifications were as follows: Met oxidation, loss and/or acetylation of protein N-terminal Met, peptide N-terminal Glu conversion to pyroglutamate, dead-end DSS modification at Lys and protein N-terminus or dead-end SIAB modification of Cys, and incorrect monoisotopic peak assignment (neutral loss of 1 Da). Up to three variable modifications per peptide were allowed. Crosslinked matches were classified using Touchstone (in-house R package, *manuscript in development*) with a minimum peptide length of three amino acids and minimum score difference of 0. Crosslinks were reported at the unique-residue pair level with 1% FDR. When crosslinks could not be uniquely identified, all possible hits were reported (supplemental Table S4).

Experimental Design and Statistical Rationale

The goal of the IκBα-APEX proteomic experiments was to identify proteins that interact with IκBα and the changes in these interactions upon p62 coexpression. We first used the SAINTexpress software package (32) to independently identify proteins specifically labeled by APEX2-IκBα with or without p62-Myc coexpression using GFP-IκBα (C1-IκBα) with p62-Myc coexpression as the negative control (Fig. 6A). Four biological replicates were performed for each condition. The Protein Prospector search results (supplemental Table S1) were reformatted and analyzed by SAINTexpress on the CRAPome website (www.crapome.org) (33). The SAINT output (supplemental Table S2) was first filtered by Bayesian False Discovery Rate score; proteins with a Bayesian False Discovery Rate score below a threshold of 0.01 in either APEX2-IκBα with p62-Myc or APEX2-IκBα without p62-Myc coexpression were retained. Average fold change values were calculated from the spectral counts of APEX2-IκBα + p62-Myc *versus* APEX2-IκBα alone, and *p*-values were calculated by a *t* test, to generate the volcano plot (Fig. 6*B*). Selected proteins that showed a significant change upon p62-Myc coexpression were searched using MaxQuant (34) for more accurate label-free intensity-based quantification (supplemental Table S3). The intensities were then normalized using IκBα intensities in each sample to generate the bar charts (Fig. 6, *C–G*).

RESULTS

Intimate Protein–Protein Interactions of p62 With IκBα Enhances Its Proteolytic Stability

Cotransfection of HEK293T cells with Myc-tagged p62 (p62-Myc) plasmid coupled with HA-tagged IκBα (HA-IκBα) plasmid and subsequent anti-Myc IgG-immunoprecipitation of the cell lysates led to the co-immunoprecipitation (co-IP) of HA-IκBα, attesting to an intimate intracellular interaction of the two proteins (Fig. 1*A*). We also found that cotransfection of the two plasmids at 1 μg each resulted in a much greater expression of IκBα protein than that observed after 2 μg transfection of HA-IκBα plasmid alone. These findings suggested that upon coexpression, p62 could be either enhancing IκBα synthesis or protecting IκBα from degradation. To directly assess the role of p62 in IκBα protein stability, we carried out cycloheximide pulse-chase analyses in HEK293T cells either expressing HA-IκBα alone or coexpressing both HA-IκBα and p62-Myc. p62 coexpression indeed extended the cellular IκBα $t_{1/2}$ from 0.25 h under basal conditions to a $t_{1/2}$ of 4.57 h, that is, an 18-fold life-span prolongation (Fig. 1*B*). This revealed that p62 enhanced IκBα cellular stability by protecting it from proteolytic turnover. Intracellular IκBα turnover involves various cellular proteolytic systems, among them the 20S/26S proteasomal and calpain systems being the most prolific under basal conditions (35–37). Thus, upon expression of IκBα alone, it was largely protected by the proteasomal inhibitor MG-132 and to a lesser extent by the calpain-inhibitor, calpeptin (Fig. 1*C*). By contrast, p62 coexpression with HA-IκBα had a major protective role that tended to minimize the additional contributions of these protease

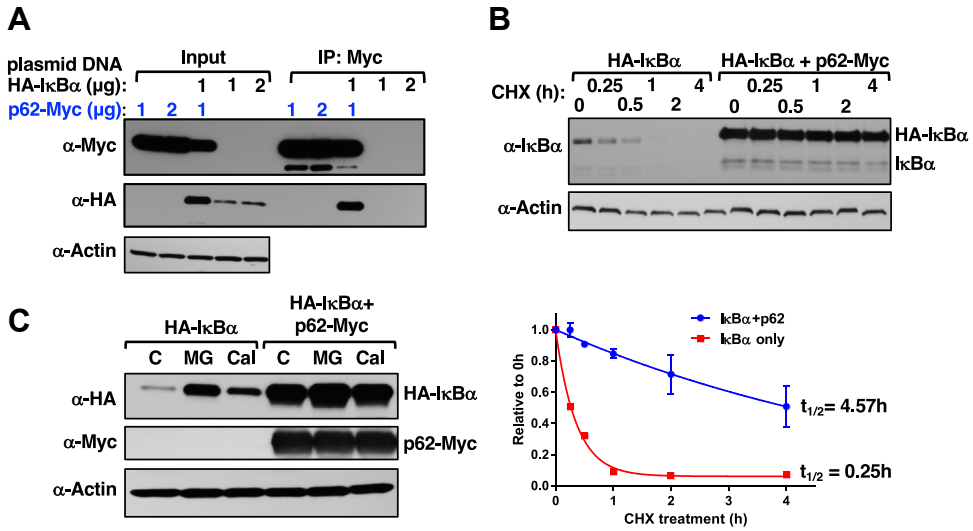

FIG. 1. **p62 stabilizes IκBα protein by blocking its proteolytic turnover.** *A*, HEK293T cells were seeded in 6-well plates overnight, and then each well was transfected with indicated amounts of pCMV4-3HA-IκBα vector (1 or 2 μg) or cotransfected with pcDNA6-p62-Myc (1 or 2 μg). Whenever necessary, pcDNA6-Myc empty vector was used to supplement such that the total plasmid DNA amount transfected was 2 μg. Forty-eight hours after transfection, cell lysates (10 μg) were used for IB analyses with actin as the loading control. *B*, HEK293T cells were transfected either alone with pCMV4-3HA-IκBα or cotransfected with pcDNA6-p62-Myc (1 μg) as in (*A*). Forty-eight hours after transfection, cells were treated with cycloheximide (CHX; 50 μg/ml) for indicated times, and cell lysates (10 μg) were subjected to IB analyses with actin as the loading control. IκBα amounts relative to 0 h control were quantified from three experimental replicates and plotted. The half-life ($t_{1/2}$) of IκBα with or without p62 coexpression was calculated based on a single exponential fit of the data with Prism Graphpad Version 6.07. *C*, HEK293T cells were transfected either alone with pCMV4-3HA-IκBα (1 μg) or cotransfected with pcDNA6-p62-Myc (1 μg) as in (*B*). Forty-two hours after transfection, cells were treated with vehicle control (*C*), or MG132 (MG; 20 μM), or calpeptin (Cal; 100 μM) for 6 h, and cell lysates (10 μg) were used for IB analyses with actin as the loading control. IκB, NF-κB inhibitor; IB, immunoblotting.

inhibitors to IκBα stability (Fig. 1*C*). Moreover, the near comparable IκBα levels upon p62 coexpression in the presence or absence of MG132 suggested that the IκBα enhancement was not due to its p62-mediated enhanced synthesis. These findings conclusively indicated that p62 interaction affords cellular protection against rapid IκBα proteolytic turnover.

Identification of the p62–IκBα Interaction Domains Through Structural Deletion, In-Cell Chemical Crosslinking/LC-MS/MS, and Site-Directed Mutagenesis Analyses

To identify the p62 subdomains involved in its IκBα interaction, we carried out p62-deletion analyses through sequential deletion of various p62-plasmid regions corresponding to structural elements that interact with various cellular protein partners and/or motifs [Phox and Bem1p-domain (PB1), Zn-finger binding motifs (ZZ), TRAF6-binding (TB), LC3-interacting region, PEST1 and PEST2 motifs, Keap1-interacting region, and Ub-association region] (15, 38–44) (Fig. 2). Each of these Myc-tagged plasmids including the WT p62-Myc plasmid was cotransfected along with the HA-IκBα plasmid into HEK293T cells, followed by p62-Myc immunoprecipitation and Western IB analyses of the coimmunoprecipitated HA-IκBα. These sequential deletion analyses identified the minimal p62 subdomain required for cellular IκBα interaction and stabilization as the N-terminal 1 to 224 (N1–224) p62 residues that contained the PB1, ZZ, and the intervening region (IR) between the ZZ and TB subdomains (Fig. 2). The C-terminal domain beyond the TB subdomain was not required for this interaction.

To identify the hotspots of p62-mediated IκBα-recognition within this N1–224 subdomain under physiological conditions, we carried out in-cell chemical crosslinking of HEK293T cells overexpressing HA-IκBα and p62-Myc using a cell-permeable chemical crosslinker either to crosslink amines to sulfhydryls, SIAB (0.05 mM), or amines to amines, DSS (0.05 mM) (Fig. 3*A*). The cells were lysed with denaturing RIPA buffer to disrupt native (noncrosslinked) protein–protein interactions. To obtain highly enriched crosslinked p62-IκBα species, the cleared RIPA lysates of DSS- or SIAB-treated cells were subjected to a dual immunoprecipitation: first with Myc-trap to pull-down p62-Myc and subsequently with anti-HA-agarose. The tandem immunoprecipitated eluates along with an aliquot of their parent lysate were then subjected to SDS-PAGE (Fig. 3*C*), two-color Western IB analyses of p62 and IκBα species followed by IR fluorescence detection (Fig. 3*B*). Overlap of the immunoblot fluorescence signals detected with either IRDye 680RD goat anti-mouse IgG (p62-Myc) or IRDye 800CW goat anti-rabbit IgG (HA-IκBα) enabled the visualization of the SIAB-crosslinked p62-IκBα species as yellow bands with molecular masses corresponding to the heterodimeric (1:1) ≈150 kDa species, as well as additional heterooligomeric

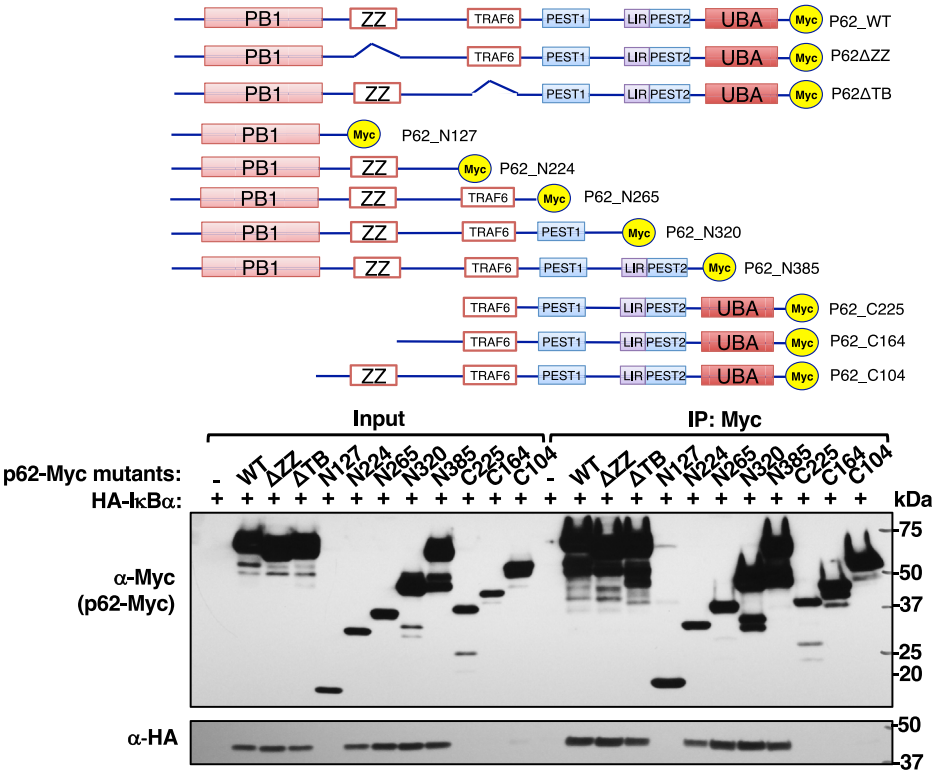

web 4C/FPO

FIG. 2. **p62-PB1 domain and p62-linker between ZZ- and TRAF6-domains are both important for IκBα stabilization.** p62 deletion and truncation mutations were constructed as schematically shown. HEK293T cells were seeded in 6-well plates overnight, and then each well was cotransfected with pCMV4-3HA-IκBα (1 μg) and either WT or indicated mutant pcDNA6-p62-Myc vector (1 μg) for 48 h. Whole cell lysates (500 μg) were used for co-IP with Myc-trap (50 μl), followed by IB analyses with HA- and Myc-antibodies. co-IP, coimmunoprecipitation; IκB, NF-κB inhibitor; IB, immunoblotting.

crosslinked species at higher (>150 kDa) molecular masses (Fig. 3*B*). Similar analyses were also carried out with DSS (Fig. 3*D* and supplemental Fig. S1). The gel-bands corresponding to these crosslinked p62-IκBα species were excised and subjected to in-gel digestion and LC-MS/MS analyses of the resulting crosslinked peptides. While p62 and IκBα were by far the most abundant endogenous proteins detected in these gel bands, potential crosslinks were searched against all proteins detected in the top two orders of magnitude with respect to abundance. A number of p62 crosslinks were discovered on a short peptide ^{187}KVK^{189}. Due to its length, it is difficult to unambiguously assign these crosslinks to p62 rather than to alternative sequences. For instance, hnRNP R peptide ^{370}VKK^{372} in the DSS bands can only be distinguished by a single y_2-ion, and UBA52 peptide ^{126}KVK^{128} in the SIAB bands is identical to the p62 sequence. All redundant explanations of these crosslinks are listed in supplemental Table S4 and the corresponding spectral annotations are available online. However, we note that the crosslinked peptides originate from gel bands which have been doubly selected for p62–IκBα interactions and further, p62 is detected at ~20 and ~100× higher NSAF levels than UBA52 and hnRNP R in these bands. Furthermore, only peptides from the Ub-domain of UBA52 were otherwise detected, while the KVK peptide is at the C-terminus of UBA52. Therefore, it is likely that p62 protein inference is correct for crosslinked peptides containing this sequence, as subsequently verified through our site-directed mutagenesis analyses of this p62 subdomain (*see below*). Two SIAB-crosslinked peptides were detected (Table 1), one between IκBα-Cys$_{239}$ in its fifth ankyrin-repeat (AR5) and p62-K$_{13}$ in its PB1 subdomain, and the other between IκBα-Cys$_{239}$ and p62-K$_{187}$ in the IR between its ZZ and TB subdomains, consistent with the SIAB ability to crosslink Lys and Cys residues (Fig. 3*D* and supplemental Fig. S2*A*). While similar DSS-crosslinked p62-IκBα species were also found, we found that the detection of these DSS-crosslinked species was greatly enhanced upon intracellular pretreatment with NEM (10 mM; 5 min) before cell harvest, followed by NEM (10 mM) addition to the lysates (supplemental Fig. S3, *D* and *E*). With this NEM pretreatment, the optimal DSS in-cell crosslinking concentration was found to be 0.05 mM, just 1% of that recommended in the manufacturer's instructions (supplemental Fig. S3*E*). Both NEM pretreatments greatly enhanced p62–IκBα interactions (supplemental Fig. S3*A*). Most likely, such NEM-elicited enhancement of DSS-mediated crosslinking was plausibly due to its maximizing available free K-residues by preventing their intracellular ubiquitination and/or sumoylation. Indeed, intracellular NEM

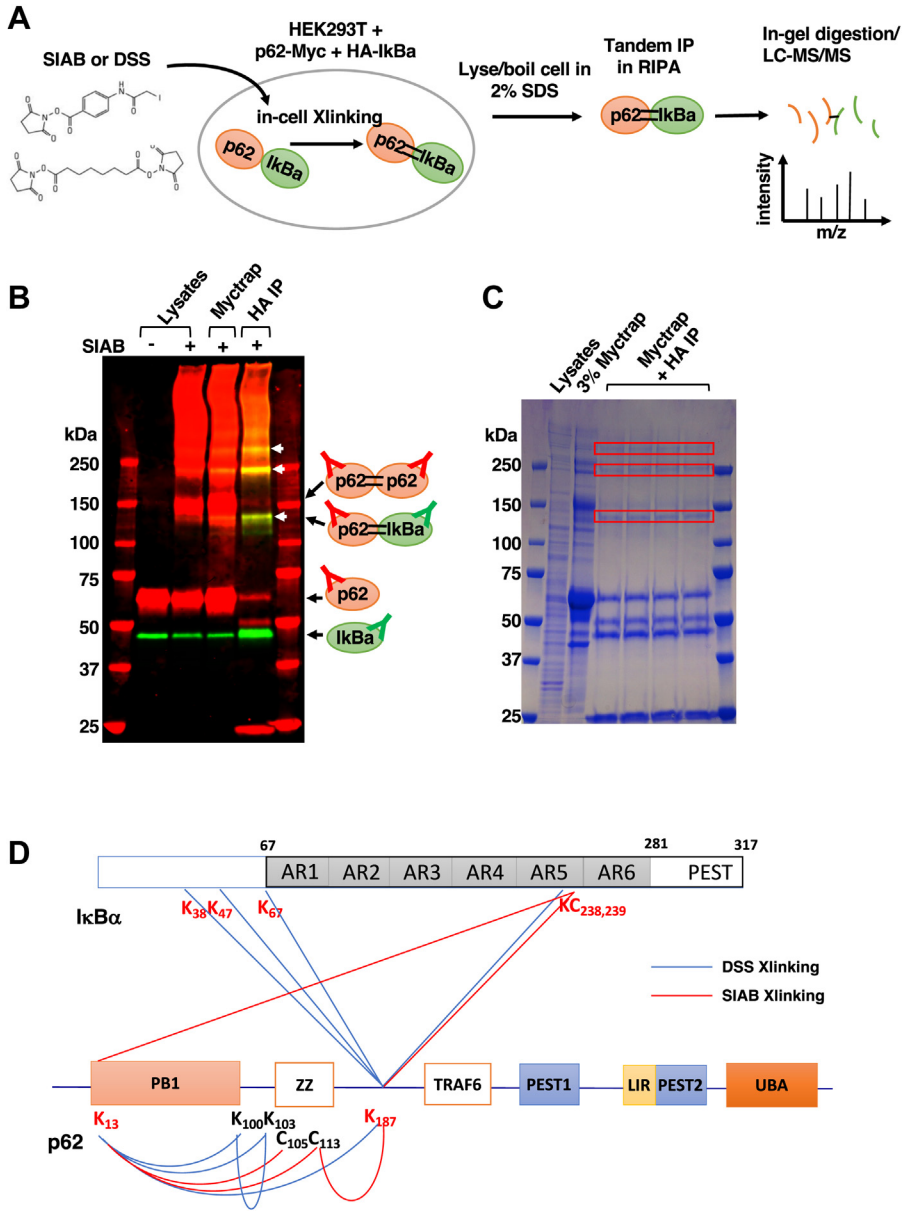

FIG. 3. **Potential p62–IκBα interaction hotspots identified by in-cell chemical crosslinking and mass spectrometric analyses.** *A*, workflow for p62-IκBα in-cell chemical crosslinking for mass spectrometric analyses. *B*, representative Western IB analyses of p62-Myc and HA-IκBα after in-cell chemical crosslinking with 0.05 mM SIAB and tandem IP, first with Myc-trap followed by HA-agarose. Crosslinked species were enriched after tandem IP, as indicated by *white arrows*. *C*, representative SDS-PAGE from large scale in-cell chemical crosslinking with 0.05 mM SIAB and tandem IP. Bands excised for in-gel digestion and LC-MS/MS are indicated by the *red boxes*. *D*, summary of inter- and intra-crosslinked sites between p62-IκBα upon DSS- and SIAB-mediated crosslinking. IκB, NF-κB inhibitor; IB, immunoblotting; DSS, disuccinimidyl suberate; SIAB, succinimidyl (4-iodoacetyl)aminobenzoate.

treatment consistent with its SH reactivity completely aborted all cellular protein ubiquitination and much of the nuclear sumoylation, further enhancing these p62–IκBα interactions (supplemental Fig. S3*B*). NEM was however incompatible with SIAB crosslinking due to its well-recognized Cys/SH-reactivity (supplemental Fig. S3*D*).

Similar in-gel digestion and LC-MS/MS analyses of the enriched immunoprecipitated DSS-crosslinked p62-IκBα species (supplemental Fig. S4) yielded four DSS-crosslinked peptides (Table 1). All these peptides documented interactions of K_{187} in the p62 IR with various IκBα K-residues residing in its N-terminus (K_{38}, K_{47}, K_{67}) as well as K_{238}, contiguous to the previously identified SIAB-crosslinked C_{239} in its AR5 (Fig. 3*D*). Coexpression of an IκBα mutant $K_{238}R$ with p62-Myc stabilized the basal IκBα–p62 interaction over that with the WT IκBα, and this interaction was further

TABLE 1
Crosslinked p62-IκBα peptides detected upon LC-MS/MS analyses

p62 peptide	IκBα peptide	Xlinked AA	Xlinked AA
AYLLGK(+SIAB)EDAAR	C(+SIAB)GADVNR	K13	C239
K(+SIAB)VK	C(+SIAB)GADVNR	K187	C239
K(+DSS)VK	GSEPWK(+DSS)QQLTEDGDSFLHLAIIHEEK	K187	K67
K(+DSS)VK	TALHLAVDLQNPDLVSLLLK(+DSS)C(NEM)GADVNR	K187	K238
K(+DSS)VK	HDSGLDSM(Oxidation)KDEEYEQM(Oxidation)VK(+DSS) ELQEIR	K187	K47
K(+DSS)VK	HDSGLDSM(Oxidation)K(+DSS)DEEYEQMVK	K187	K38
p62 peptide	**p62 peptide**		
AYLLGK(+DSS)EDAAR	IYIK(+DSS)EK	K13	K100
IYIK(+DSS)EK	K(+DSS)EC(N-ethylmaleimide)R	K100	K103
AYLLGK(+DSS)EDAAR	K(+DSS)EC(N-ethylmaleimide)R	K13	K103
AYLLGK(+DSS)EDAAR	EK(+DSS)K	K13	K102
AYLLGK(+DSS)EDAAR	AYLLGK(+DSS)EDAAR	K13	K13
AYLLGK(+SIAB)EDAAR	DHRPPC(+SIAB)AQEAPR	K13	C113
AYLLGK(+SIAB)EDAAR	EC(+SIAB)R	K13	C105
RDHRPPC(+SIAB)AQEAPR	K(+SIAB)VK	C113	K187

enhanced when an IκBα mutant (9KR) with all its nine K-residues mutated to R was coexpressed (supplemental Fig. S3*C*). These findings suggest that (i) a positively charged IκBα K or R residue is involved in these interactions, and (ii) in these p62–IκBα interactions, an R-residue is apparently favored over K, plausibly by circumventing posttranslational K-modifications that would disrupt these interactions.

Together, the above XLMS analyses reveal that the N-terminal p62 domain (N1–224) forms important interactions with two IκBα-subdomains: One in its N-terminus (encompassing K_{38}, K_{47}, and K_{67}) and the other in its C-terminal AR5 (around K_{238}/C_{239}). The latter site is in close proximity to AR6 (residues 243–280), which apparently harbors a degron (residues 251–262) for Ub-independent proteasomal degradation of IκBα (36).

To further define the importance of these p62 subdomains to its IκBα interaction, we carried out site-directed mutagenesis of p62 residues flanking K_{13} and K_{187} followed by a HEK293T cell cotransfection of Myc-tagged constructs and an anti-Myc immunoprecipitation approach similar to that used above (Fig. 2). These findings revealed that mutation of p62 residues L_{10}/L_{11}, K_{13}, or D_{14}/E_{15} to Ala had very little influence on its IκBα–protein interactions (Fig. 4). On the other hand, mutation of p62 residues W_{184}/L_{185} and K_{187}/K_{189} to

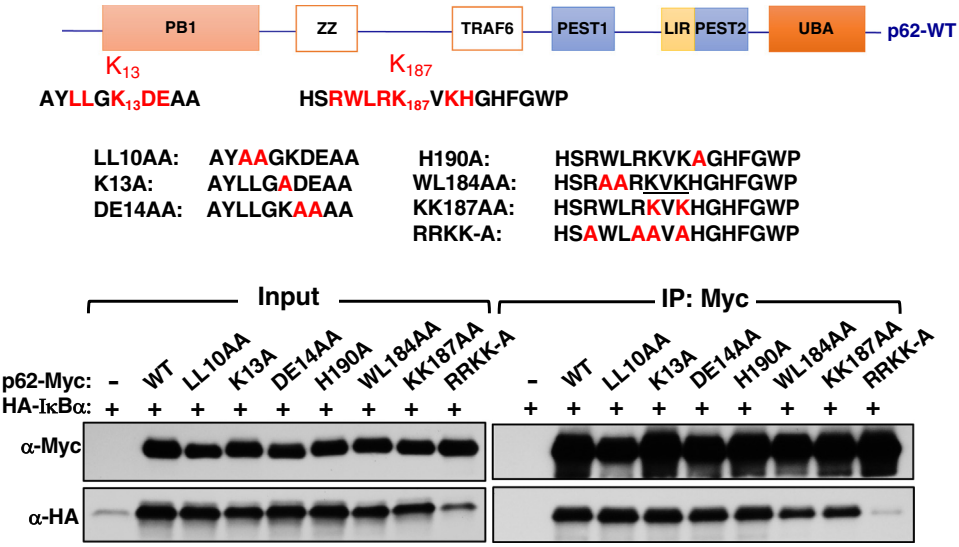

FIG. 4. **p62–IκBα interaction sites identified by site-directed mutagenesis.** Potential sites in p62 identified as IκBα-interaction hotspots (Fig. 3) were mutated to alanine as shown schematically. HEK293T cells were seeded in 6-well plates overnight, and then each well was cotransfected with pCMV4-3HA-IκBα (1 μg) and either WT or indicated mutant pcDNA6-p62-Myc (1 μg) for 48 h. Whole cell lysates (500 μg) were used for co-IP with Myc-trap (50 μl), followed by IB analyses with HA- and Myc-antibodies. co-IP, coimmunoprecipitation; IκB, NF-κB inhibitor; IB, immunoblotting.

ALA reduced its IκBα–protein interactions, while that of H_{190} had little effect. By contrast, mutation of p62 residues R_{183}/R_{186}/K_{187}/K_{189} flanking its IκBα-crosslinked K_{187} site completely aborted this interaction (Fig. 4), thereby identifying this positively charged p62-microregion as a hotspot for IκBα interaction.

To identify the corresponding IκBα hotspots involved in its p62 interactions, we carried out IκBα-structural deletion analyses (Fig. 5). For reference, IκBα–NF-κB interactions under basal conditions are depicted (Fig. 5*A*; (45)). Given that the positively charged p62 microregion is a hotspot for IκBα interaction, we aimed at identifying negatively charged IκBα

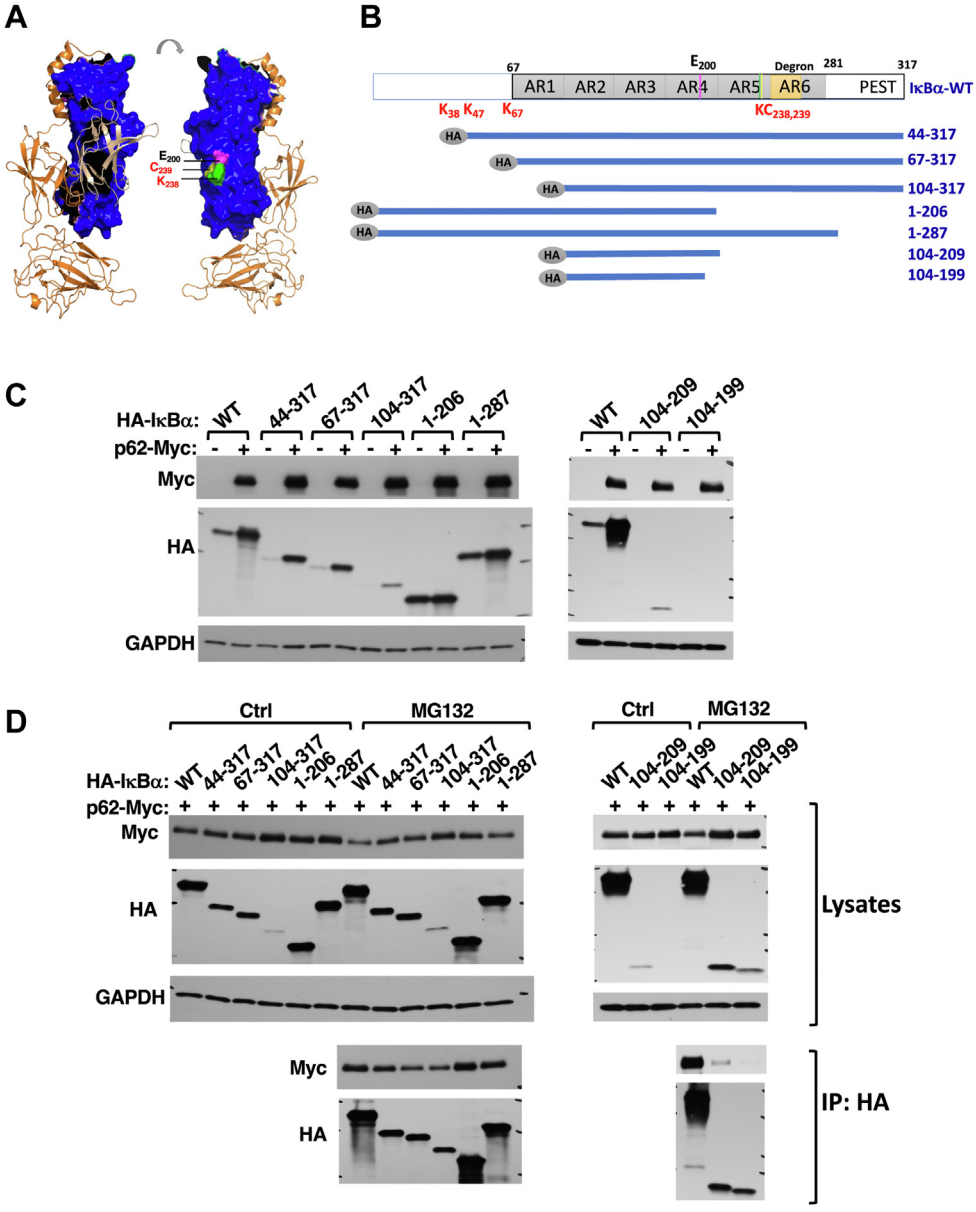

FIG. 5. **IκBα p62-interaction region verified by structural mutagenesis.** *A*, crosslinked sites (*green*) and the negatively charged amino acids adjacent to the crosslinked sites (*magenta*) are highlighted on the surface of the IκBα structure (*blue*) complexed with p65-p50 (depicted as *orange ribbon*). *B*, scheme of a series of N-terminal and C-terminal truncation mutants of IκBα were designed and constructed corresponding to the hotspots identified (Figs. 3 and 4). *C*, HEK293T cells were seeded in 6-well plates overnight, and then each well was transfected with pCMV4-3HA-IκBα WT or indicated mutants (1 μg) with or without pcDNA6-p62-Myc for 48 h. Whole cell lysates (10 μg) were subjected to IB analyses with GAPDH as the loading control. *D*, HEK293T cells were seeded in 6-well plates overnight, and then each well was cotransfected with pCMV4-3HA-IκBα WT or indicated mutants (1 μg) along with pcDNA6-p62-Myc for 42 h. Cells were treated with vehicle control (0.05% methanol) or MG132 (20 μM) for 6 h. Whole cell lysates (500 μg) were used for co-IP with HA-agarose (50 μl), and eluates as well as cell lysate input (10 μg) were used for IB analyses with HA- and Myc-antibodies. co-IP, coimmunoprecipitation; IκB, NF-κB inhibitor; IB, immunoblotting.

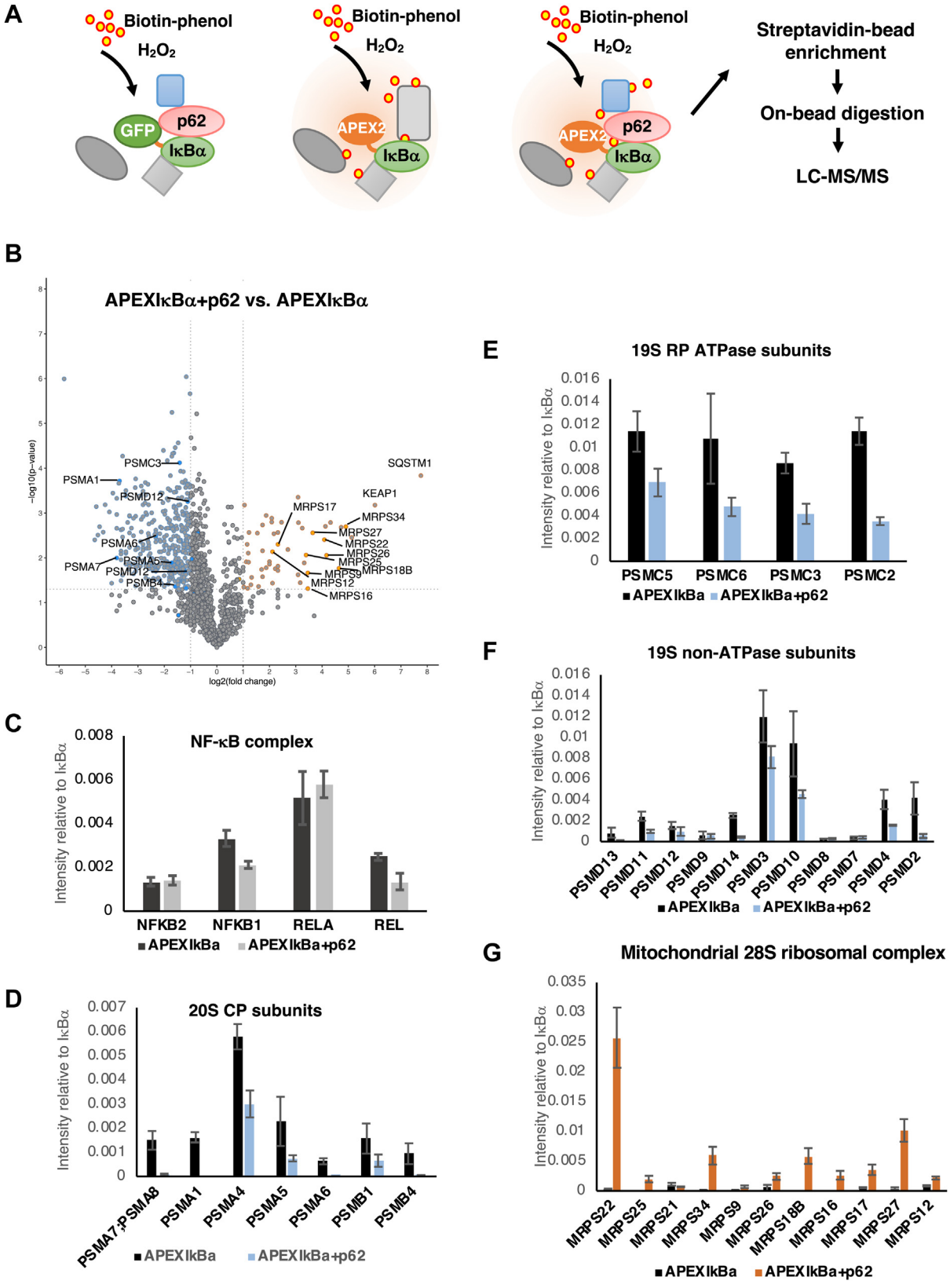

web 4C/FPO

FIG. 6. **APEX captures proteins that differentially interact with IκBα upon p62 coexpression.** *A*, scheme of APEX workflow to identify and compare proteins that specifically interact with IκBα when it was expressed alone or when it was coexpressed with p62. GFP-IκBα was used as a

residues either adjacent or in the vicinity of its p62-crosslinked K or C residues on the IκBα structural surface. As depicted in magenta (Fig. 5*A*), two plausible negatively charged sites were identified: $E_{85}E_{86}$ close to K_{67} and E_{200} adjacent to K_{238} (supplemental Fig. S5). Individual site-directed mutation of each of these E-residues to Ala failed to appreciably alter p62–IκBα interactions (*Data not shown*). We then designed IκBα-truncation mutants to sequentially delete domains containing these plausible p62-interaction hotspots. In these analyses, plasmid constructs encoding various HA-tagged IκBα subdomains (depicted in Fig. 5*B*) were cotransfected into HEK293T cells with or without the p62-Myc plasmid (Fig. 5*C*). To assess the extent of p62 protection against IκBα proteasomal degradation, and to maximize the detection of IκBα levels through stabilization, these cells were also pretreated with or without the proteasomal inhibitor MG-132 (Fig. 5*D*). Cells coexpressing HA-IκBα and p62-Myc were then subjected to anti-HA co-IP to determine the amount of interacting p62 as in Figure 1*A*. Relative to the WT protein, IκBα proteins with deletions of its PEST subdomain and/or the Ub-independent degradation degron (constructs 1–206 and/or 1–287) were inherently more stable, but p62 coexpression further enhanced their stability, and MG-132 had minimal further effect. IκBα proteins with substantial deletions of the N-terminal residues (constructs 44–317, 67–317, 104–317), were inherently less stable, but their stability was greatly rescued by p62 coexpression, with minimal further effect by MG132 treatment (Fig. 5*C*). This suggested that p62 could still interact and stabilize IκBα with either the C-terminal AR5, AR6, and PEST domains deleted or the N-terminal regulatory region and AR1 domains deleted. By contrast, the IκBα proteins with both N- and C-terminal regions deleted (constructs 104–199 and/or 104–209) and thus excluding all the potential p62-interaction sites were inherently unstable, and p62-coexpression failed to rescue these proteins. Only cell treatment with MG132 was capable of appreciably stabilizing these two truncation mutants. Remarkably, construct 104 to 199, with E_{200} deleted, totally lacked its p62-mediated stabilization (Fig. 5*C*, *right panel*) and interaction, even in the presence of MG132 (Fig. 5*D*, *lower right*, *IP/HA data*). Together, these findings (Figs. 4 and 5) reveal that IκBα-protein stability and molecular p62-IκBα-protein interactions not only rely on both N- and C-terminal IκBα-subdomains but are also largely dependent on the positively charged p62 residues in its IR subdomain. Inspection of the existing crystal structure of the IκBα–NF-κB complex ((45); Fig. 5*A*) reveals that these p62-interacting IκBα regions are on the IκBα-interface opposite to that which binds NF-κB (45–47) and thus are not expected to competitively disrupt its NF-κB association.

Influence of p62–IκBα Interactions on Intracellular IκBα-Protein Partnerships as Monitored Through In-Cell APEX-Proximity Labeling Analyses

The collective findings of the sequence-deletion analyses coupled with the finding that some mutant IκBα proteins (*i.e.*, constructs 104–199 and 104–209) found incapable of significant p62 interaction, could be appreciably stabilized only by MG-132 but not by p62-coexpression (Fig. 5*D*), indicated that efficient p62 interaction affords cellular protection against rapid IκBα-proteolytic turnover and could thus effectively influence its cellular function and partnerships.

To scrutinize these cellular p62-IκBα-protein interactions in greater detail and elucidate additional participants and/or interacting partners if any, we conducted in-cell APEX-proximity labeling analyses. Our aim was to determine the relative differences in the IκBα interactome with or without p62 coexpression. We compared APEX-IκBα fusion–labeled biotinylated proteins with or without p62 coexpression, after filtering out the nonspecific binders by employing GFP-IκBα coexpressed p62 as a negative control (Fig. 6*A* and supplemental Fig. S6).

Not surprisingly, Volcano plot analyses of cells coexpressing both APEX-IκBα and p62-Myc relative to those expressing APEX-IκBα alone revealed that upon p62 coexpression, many cellular interactants were either significantly increased or decreased several-fold (Fig. 6*B*). However, consistent with the p62 interaction with residues on the IκBα-interface opposite to that of its NF-κB interaction, p62 coexpression did not appreciably affect IκBα-associated NF-κB2 (p52) and RelA (p65) levels, whereas NF-κB1 (p50) and Rel C levels were only slightly (<2-fold) reduced (Fig. 6*C*). By contrast, the levels of several 19S proteasomal regulatory particle ATPase and non-ATPase subunits as well as 20S proteasomal core subunits interacting with IκBα were markedly reduced upon p62 coexpression (Fig. 6, *D–F*), quite consistent with the impaired

negative control for APEX-labeling. *B*, volcano plot of relative protein spectral count derived from APEX-IκBα and APEX-IκBα + p62 proteomic analyses. Data from four independent experiments are presented as the mean. Proteins found to interact to a greater extent with IκBα when p62 is present are highlighted in *orange* (Fold change > 2, p value < 0.05), proteins found to interact to a greater extent with IκBα when p62 is absent are highlighted in *blue* (Fold change > 2, p value < 0.05). *C*, bar chart of the relative intensities of identified NF-κB complex proteins derived from APEX-IκBα and APEX-IκBα + p62 proteomic analyses. Data presented as mean ± SD (n = 4). *D*, bar chart of the relative intensities of identified 20S core proteasomal subunit proteins derived from APEX-IκBα and APEX-IκBα + p62 proteomic analyses. Data presented as mean ± SD (n = 4). *E*, bar chart of the relative intensities of identified 19S proteasomal regulatory particle ATPase subunit proteins derived from APEX-IκBα and APEX-IκBα + p62 proteomic analyses. Data presented as mean ± SD (n = 4). *F*, bar chart of the relative intensities of identified 19S regulatory particle non-ATPase subunit proteins derived from APEX-IκBα and APEX-IκBα + p62 proteomic analyses. Data presented as mean ± SD (n = 4). *G*, bar chart of the relative intensities of identified mitochondrial 28S ribosomal complex proteins derived from APEX-IκBα and APEX-IκBα + p62 proteomic analyses. Data presented as mean ± SD. IκB, NF-κB inhibitor.

proteasomal degradation and greater proteolytic stability observed upon its cellular p62 interaction. On the other hand, the interactions of the IκBα–p62 complex with the mitochondrial 28S ribosomal complex tended to increase (Fig. 6*G*), suggesting greater IκBα localization to the mitochondrial matrix, possibly due to enhanced intramitochondrial p62-mediated IκBα-trafficking.

Disruption of Intracellular p62-IκBα Protein Interactions: Physiological and Pathophysiological Consequences

Collectively, the above findings revealed that by influencing IκBα proteolytic stability, p62 could regulate the relative robustness of the cellular NF-κB-IκBα association and consequently NF-κB activation (Fig. 7). To probe any such potential p62 regulation, we first examined TNFα-elicited NF-κB activation and subsequent feedback termination in WT and $p62^{-/-}$-MEF cells (Fig. 8*A*). In WT MEF cells, TNFα treatment elicited rapid destruction of the cytoplasmic NF-κB–associated IκBα, followed by unleashing of NF-κB, its nuclear translocation (as evidenced by the increased nuclear p65 content), and its activation (reflected by the increased nuclear phosphorylated p65 (P-p65) content). The consequent transcriptional activation of the NF-κB-target IκBα gene resulted in rapid *de novo* IκBα protein synthesis that effectively terminated the TNFα-elicited NF-κB activation (evidenced by decreased nuclear p65 and P-p65 content), consistent with a classical NF-κB-IκBα negative feedback loop (9, 11). By contrast, in $p62^{-/-}$-MEF cells, the newly synthesized IκBα pool being much more labile in the absence of p62 was unable to vigorously strip the DNA-associated NF-κB and escort it out of the nucleus, thus disrupting the NF-κB-IκBα negative feedback loop. As a result, NF-κB persisted in the nucleus and its activation was greatly prolonged (Fig. 8*A*).

Similar disruption of the NF-κB-IκBα negative feedback loop was also observed in $p62^{-/-}$-HepG2 cells (Fig. 8*B*) upon stimulation with IL-1β, another inflammatory cytokine that is a more potent NF-κB transcriptional activator than TNFα in HepG2 cells and mouse liver hepatocytes (supplemental Fig. S7*A*). In these IL-1β–stimulated $p62^{-/-}$-HepG2 cells, the lack of p62-mediated stabilization caused greater proteolytic degradation of the newly synthesized IκBα, which could be prevented by MG132 treatment (Fig. 8*C*, *cytosolic extract (CE) panel*). As a result, the nuclear NF-κB activation (P-p65) and persistence was prolonged relative to those in the corresponding $p62^{+/+}$-WT cells (Fig. 8*B* and supplemental Fig. S7*B*), establishing that p62 was indeed required for a robust NF-κB-IκBα negative feedback loop response. These findings of proteolytic loss of the newly synthesized IκBα and the greater NF-κB nuclear persistence could also be documented through confocal immunofluorescence microscopic analyses in IL-1β–stimulated $p62^{-/-}$-HepG2 cells relative to corresponding WT cells (supplemental Fig. S8).

To further verify the physiological and pathophysiological relevance of intact p62–IκBα interactions *in vivo*, we generated a mutant mouse upon liver-specific genetic ablation of the p62 residues 68 to 252 (p62mut). This p62mut thus lacks among other p62 subdomains such as its OPCA motif, the critical hepatic IκBα-p62 interacting region (IR, R_{183}, R_{186}, K_{187}, and K_{189}) (Fig. 9*A*). However, this p62mut retains not only its LC3-interacting region domain but also surprisingly its capacity to oligomerize given its ability to form autophagic puncta upon LC3 recruitment and thus functioning in its normal capacity as an autophagic receptor (supplemental Fig. S9). After IL-1β

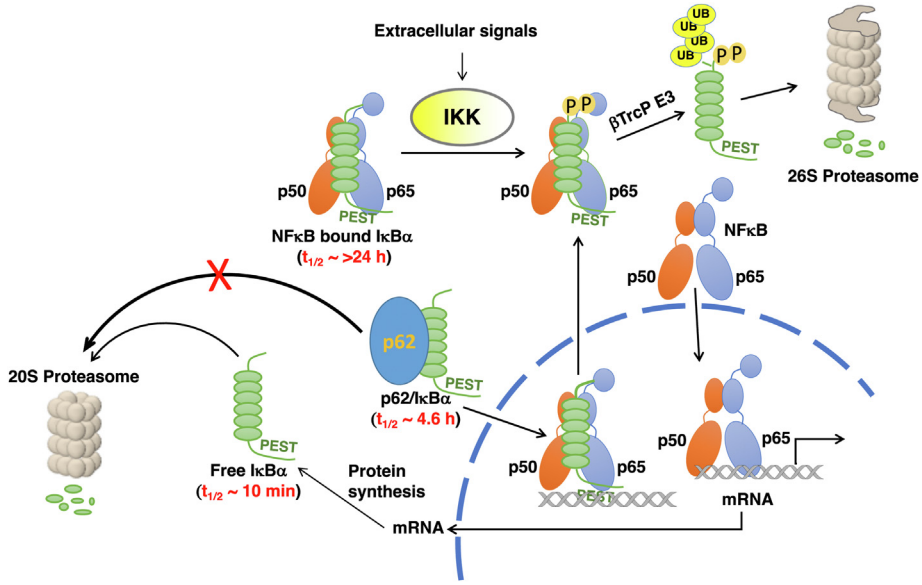

FIG. 7. **A scheme of the cellular pathway of NF-κB activation and IκBα-mediated feedback loop, indicating a potential role of p62 in IκBα-stabilization and IκBα-feedback.** IκB, NF-κB inhibitor; NF-κB, nuclear factor kappa-light-chain-enhancer of activated B cells.

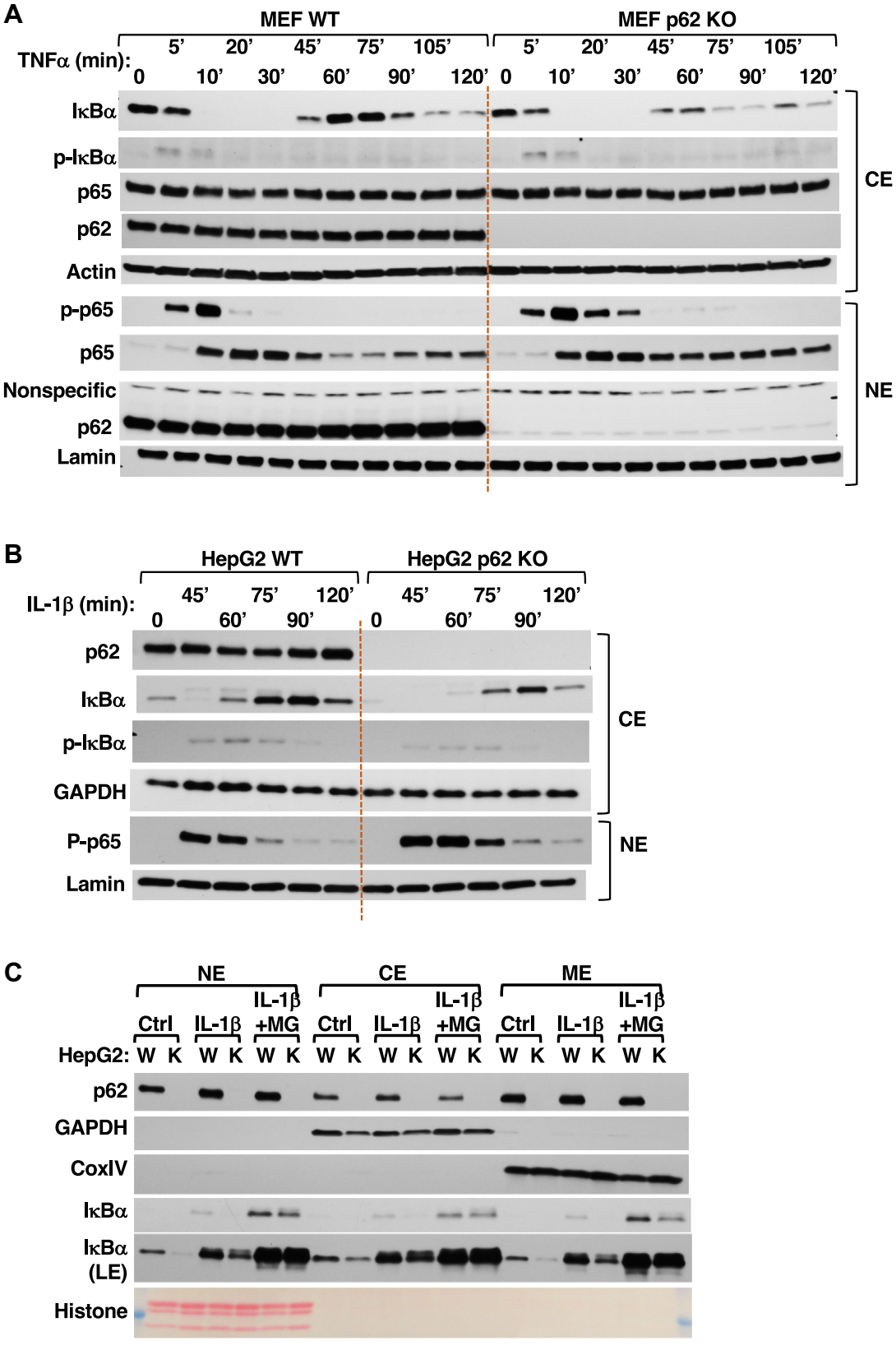

web 4C/FPO

FIG. 8. **p62-KO resulted in more intense and prolonged NF-κB response.** *A*, p62 WT and KO MEF cells were stimulated with TNFα (20 ng/ml). Cells were collected at indicated times and fractionated into cytoplasmic extracts (CEs) and nuclear extracts (NEs). Extracts (10 μg) were

stimulation of p62mut mouse hepatocytes with disrupted p62–IκBα interactions (Fig. 9*B*), a similarly reduced level of newly synthesized IκBα along with a prolonged nuclear NF-κB (P-p65) activation was observed as in p62$^{-/-}$-HepG2 cells (Fig. 8*B*). Liver histological analyses revealed that while the WT mice exhibited an age-dependent mild hepatic inflammation, this was considerably further exacerbated in the p62mut mice, effectively leading to their increased mortality by 16 months of age (Fig. 9*C*). Such age-dependent relative increases in liver inflammation in p62mut mice were associated with corresponding increases in their hepatic levels of inflammatory markers [IL-6, IL-1β, TNFα, and SPP-1 (osteopontin/secreted phosphoprotein 1)] over age-matched WT controls (supplemental Fig. S10). These findings conclusively established that disruption of physiological p62-IκBα interactions has severe pathophysiological consequences.

DISCUSSION

Collectively, our findings detailed above reveal an intimate intracellular p62-IκBα association, which stabilizes cellular IκBα levels by limiting its interaction with the 20S/26S proteasome and subsequent degradation, thereby greatly extending its life-span. The enhancement of such interactions upon cell/lysate pretreatment with NEM which would abrogate SH-elicited posttranslational modifications such as ubiquitination and/or sumoylation suggests that p62 preferentially interacts with the native, unmodified IκBα, thus possibly favoring the nascent, *de novo*–synthesized protein.

Our characterization of such p62–IκBα interactions through various complementary approaches such as structural deletion, in-cell XLMS, and/or site-directed mutagenesis analyses of each protein as well as cell transfection/co-IP assays have revealed structural hotspots critical to this protein–protein interaction. Intriguingly, our Alpha-Fold 2 structural analyses of the p62–IκBα complex predicted similar molecular interactions, thus independently reinforcing our findings (Fig. 10). Thus, in p62, the basic residues (R_{184}, R_{186}, K_{187}, and K_{189}) appear critical for its IκBα association, as this association is nearly abrogated upon their Ala mutation. Intriguingly, this p62 site coincides with its designated NLS1 (residues 183–194) (42). Although chemical crosslinking also revealed IκBα interactions with p62 K_{13}, Ala mutation of this residue and/or its neighboring residues (L_{10}, L_{11}, D_{14}, E_{15}) failed to appreciably affect p62-IκBα interactions (Fig. 4). Similar IκBα analyses identified two major hotspots: one in its N-terminus centered around residues 38 to 67, and the other around residues 238/239 in its fifth AR-domain (ARD). The sufficiently close proximity of the latter p62-crosslinked site to its Ub-independent degron (residues 243–280) in its sixth ARD (36), which is normally masked through NF-κB binding, most likely accounts for the IκBα proteolytic stability conferred by both p62 as well as NF-κB association. However, following proinflammatory stimulation of nuclear NF-κB activation, this degron in *de novo*–synthesized IκBα protein would be unshielded and subject to rapid proteasomal degradation. Strategically, cytoplasmic association with p62, which is also concurrently induced upon NF-κB activation (13–18), would enable IκBα survival long enough to insure its nuclear import and consequent tight regulation of the relative duration of NF-κB–mediated transcriptional activation cycle. Consistently, in the absence of cellular p62, the proteolytic instability of *de novo*–synthesized IκBα resulted not only in prolonged activation of NF-κB (P-p65) but also in its nuclear persistence beyond the normal TNFα- or IL-1β–elicited IκBα-NF-κB feedback cycle (Fig. 8 and supplemental Fig. S8). Our findings would thus argue that in addition to the two cellular IκBα pools known to exist, that is, a major (≈85%), long-lived cytoplasmic NF-κB–complexed IκBα-pool ($t_{1/2}$ ≈ days) and a minor (≈15%) much shorter-lived free IκBα-pool ($t_{1/2}$ ≈ 10–15 min) (20, 35), a third cellular pool of p62-complexed IκBα ($t_{1/2}$ of ≈4.6 h) must exist to shield *de novo*–synthesized "free" IκBα from rapid proteasomal degradation, thereby enabling its nuclear import and subsequent effective negative feedback regulation of nuclear NF-κB activation. Given that the p62 interaction occurs with the IκBα interface directly opposite to that of its NF-κB binding (45–47), the possibility of p62-piggy backing with the longer lived IκBα-NF-κB pool is in principle conceivable. However, this is precluded by the fact that no NF-κB was ever detected in the DSS- or SIAB-crosslinked IκBα–p62 complexes upon our proteomic verification. More importantly, such a close p62 association with the newly synthesized IκBα would circumvent the rapid proteasomal degradation that free, nascent IκBα with its readily accessible PEST and Ub-independent and Ub-dependent degrons could otherwise be subject to (20, 35, 36). This important protective chaperone role notwithstanding, the strategic inflammatory stimuli-elicited NF-κB–mediated concurrent transcriptional activation of both p62 and IκBα (13–18), and the above documented association of these two *de novo* synthesized proteins, leads us to propose that this association may additionally enable efficient nuclear import of IκBα required to terminate the NF-κB activation cycle.

used for IB analyses. *B*, p62 WT and CRISPR-KO HepG2 cells were pulse stimulated with IL-1β (20 ng/ml) for 15 min. Cells were collected at indicated times and fractionated into CEs and NEs. Extracts (10 μg) were used for IB analyses. *C*, p62 WT (W) and CRISPR KO (K) HepG2 cells were either untreated (Ctrl) or pulse-stimulated with IL-1β (20 ng/ml) for 15 min, then incubated with or without MG132 (MG; 20 μM) for an additional 75 min. Cells were collected and then separated into NEs, CEs, and MEs. Extracts (10 μg) were used for IB analyses with GAPDH as the loading control as well as a cytoplasmic marker, histone H3 as the loading control and nuclear marker, and CoxIV as loading control and mitochondrial marker. IB, immunoblotting; LE, Longer exposure; MEF, mouse embryo fibroblast; NF-κB, nuclear factor kappa-light-chain-enhancer of activated B cells.

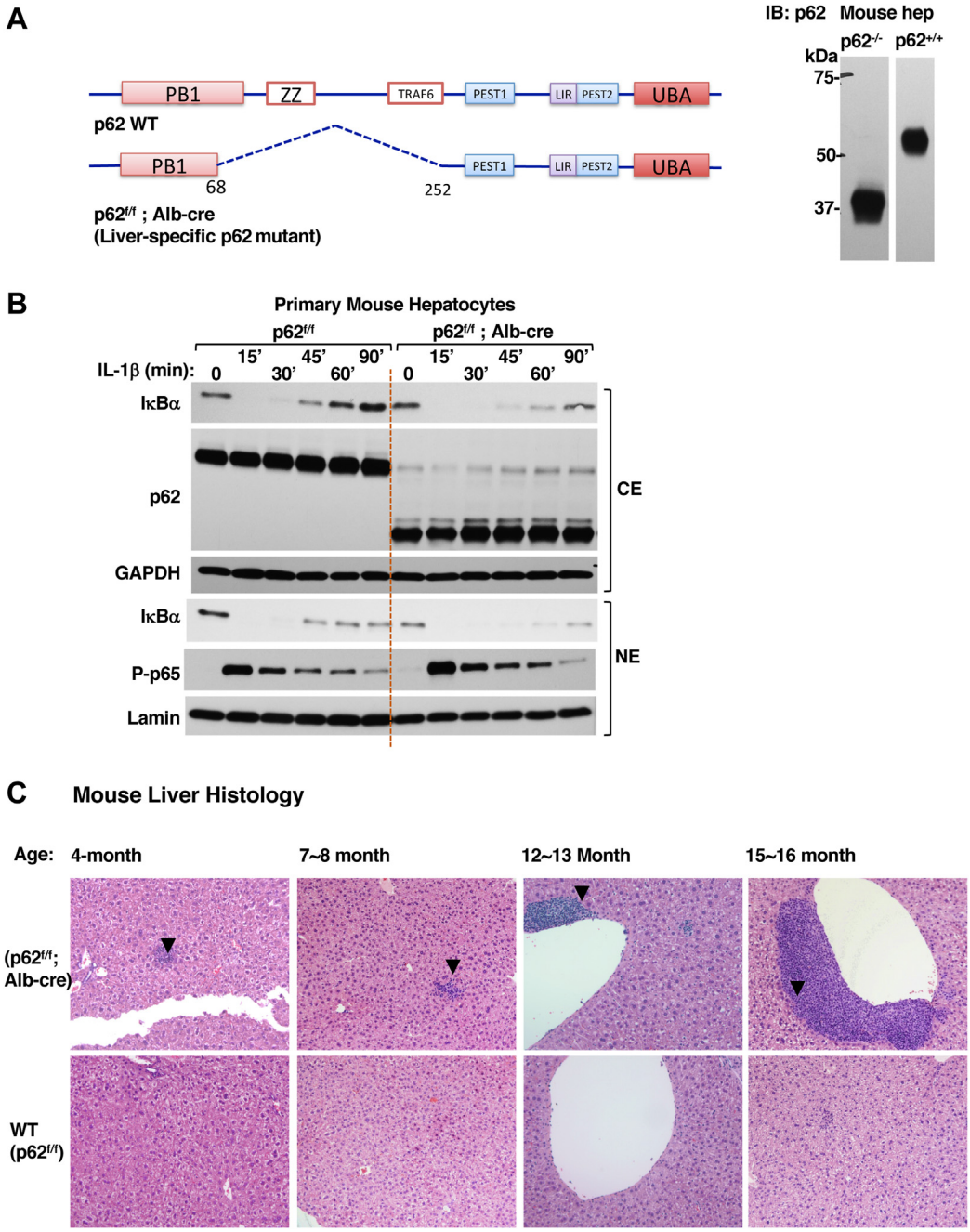

web 4C/FPO

FIG. 9. **Transgenic mice with a liver-specific p62 deletion of the IκBα-interacting region (p62mut) exhibited increased inflammation upon aging.** *A*, a scheme indicating the p62-region deleted in the liver-specific p62mut mice and p62 Western immunoblot of hepatocytes isolated from p62 WT and p62mut mice. *B*, primary hepatocytes from these WT and p62mut mice were cultured for 5 days, then pulse stimulated with IL-1β (20 ng/ml) for 15 min, and then harvested at indicated times and fractionated into cytoplasmic extracts (CEs) and nuclear extracts (NEs). Extracts (10 μg) were used for IB analyses. *C*, mice at indicated age ranges (4–16 months) were sacrificed and liver pieces were used for H&E stain and histology. *Arrows* indicate inflammatory regions. IκB, NF-κB inhibitor; IB, immunoblotting.

IκBα nuclear import given its small molecular size and lack of canonical structural NLS was once believed to occur *via* simple diffusion (9, 48). However, this view was modified when a novel class of noncanonical *cis*-acting discrete nuclear import sequences (NISs) that consist of a hydrophobic residue cluster within the IκBα-N-terminal 114 to 124 residues in its second ARD was identified as the predominant, albeit not sole NIS (49). This second ARD hydrophobic cluster is highly conserved among other IκB family proteins, and all the IκB-proteins commonly sharing this second

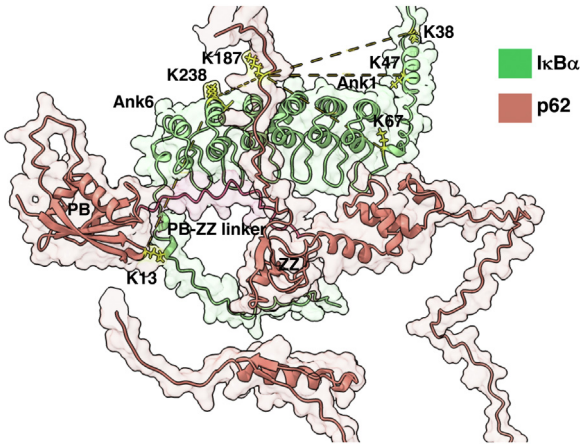

web 4C/FPO

FIG. 10. **AlphaFold 2 structural analyses predict an interaction between the p62 PB-ZZ linker and IκBα ARs.** The p62-IκBα dimer interaction was modeled using AlphaFold v2.1.2. All five of the independent modeling runs predicted similar structures with contacts between the PP-ZZ linker of p62 and 4 to 6 ARs of IκBα with Predicted Aligned Error (PAE) values between 15 and 20 Å (supplemental Fig. S11). The top ranked model is shown with the PB-ZZ linker (residues 102–123 shown in *magenta*). Crosslinked Lys-residues are shown in *yellow*. K187 on p62 occurs on a flexible loop that is poorly localized in the AlphaFold model. K13 on p62 lies in the PB-1 domain which mediates oligomerization between p62 protomers. Crosslinks between K13 and C239 are not plausible as depicted and most likely originate from a p62 oligomeric IκBα-interaction. IκB, NF-κB inhibitor.

ARD-hydrophobic cluster exhibit the apparently conserved feature of nuclear import (49). Furthermore, insertion of this ARD hydrophobic cluster into other NLS-deficient proteins confers nuclear import capabilities on them (49). Although such a nuclear import does not require Rel-proteins, this ARD hydrophobic cluster is critical both for its p65 association and blocking its DNA binding, as it is masked upon cytoplasmic p65 binding (20, 49). A fully functional AR-derived IκBα-NIS harboring such an ARD hydrophobic cluster was subsequently proposed to consist of N-terminal β-hairpin, two α-helices and N-terminal β-hairpin of the adjacent ARD (49). However, whether this discrete NIS functioned autonomously or required a piggy-back mechanism and/or another receptor that was importin-assisted remained unclear. Turpin *et al.* (50) similarly concluded that IκBα nuclear import was not *via* passive diffusion but *via* a specific active cytosol/energy-dependent process whose *in vitro* reconstitution required IκBα ARDs, Ran-GDP, α- and β-importin, and yet unknown cytosolic factor(s). Because passage of the cytosolic fraction through an affinity GST-IκBα[68–243] column but not through a GST column aborted the capacity of the cytosolic fraction to fully reconstitute the nuclear IκBα import process, they argued that ARDs contained in the IκBα[68–243] residue domain could sequester and thus effectively deplete this cytosolic factor(s) (50). By contrast, this depleted cytosolic fraction could fully support the nuclear import of a BSA-NLS-FITC protein containing a basic amino acid stretch NLS (50). This led to their proposal that most likely, IκBα nuclear import machinery additionally included an unknown cytosolic factor containing a basic NLS for piggy-backing IκBα (50). Subsequently, Lu *et al.* (51) further refined this concept and proposed a novel, importin-*in*dependent RanGDP/AR nuclear import pathway that relied on an IκBα nuclear import code: 13th hydrophobic residues of two consecutive ARs that interact with RanGDP to chaperone IκBα through the nuclear pore complex aided by specific RanGDP interactions with the FG-rich nuclear pore complex components, Nup153 and RanBP2 (52–56). These studies were largely conducted following cotransfections of these FITC-tagged AR-derived constructs into digitonin-permeabilized cells and subsequent pull-downs with GST-RanGDP (51). However, to our knowledge, intact IκBα has never been actually documented to similarly localize to the nucleus solely *via* this nuclear import pathway. Our previous proteomic findings of ZnPP aggregates revealing the existence of a very close and consistently strong association between IκBα, Nup153, and RanBP2, but not with either importin α or β, also led us to conclude that RanGDP due to its reported affinity for Nup153 and RanBP2 (49–53) was most likely involved in IκBα nuclear import (21).

However, the IκBα[68–243] domain that was suggested to sequester and thus deplete the critical cytosolic factor required for IκBα nuclear import (50) not only contains its ARDs but also regions adjacent to K_{67} as well as K_{238}/C_{239} residues we found situated in its p62-interacting hotspots. Thus, p62 could very well qualify as one, if not, the only depleted cytosolic factor. This consideration coupled with our findings described above make it plausible that p62 could represent a *bona fide* piggy-back for IκBα nuclear import. Several intrinsic features uniquely qualify p62 for such a role: (i) p62 reportedly shuttles continuously in and out of the nucleus (42). Although its NLS1 would be masked by IκBα association, its structurally more dominant basic NLS2 ($K_{264}RSR_{267}$-residues) (39), being eminently accessible, would enable participation in such nuclear import. (ii) Its NF-κB–elicited concurrent transcriptional induction with IκBα (13–18) could readily promote the association of these two *de novo*–synthesized proteins. (iii) The intimate cellular association of the two proteins and the observed considerably reduced nuclear levels of IκBα with correspondingly increased NF-κB nuclear preponderance and persistence upon p62-KO (Fig. 8 and supplemental Fig. S8). Intriguingly, in IL-1β–stimulated HepG2 cells, even though upon MG132-mediated proteasomal inhibition, cytoplasmic IκBα levels in p62-KO cells could be restored to the same level as in WT, the nuclear IκBα levels were consistently reduced in p62-KO cells relative to corresponding WT controls. This additionally argues that p62 may not solely protect IκBα against proteasomal degradation, but also function in its nuclear import. (iv) p62 interaction with the

IκBα interface opposite to that of its NF-κB interaction in such p62–IκBα complexes (45–47), far from impeding, would strategically favor IκBα hand-off for stripping the DNA-bound NF-κB required for the termination of each NF-κB activation cycle through IκBα-mediated DNA dissociation and subsequent escort out of the nucleus.

In addition to providing the much sought after "piggy-back" for IκBα nuclear import, it is plausible that p62 may similarly function in mitochondrial import of IκBα. The p62-mediated negative regulation of inflammation through mitophagy has been previously documented in macrophages (57). Our findings reveal that p62 coexpression led to increased IκBα localization to the mitochondria matrix (Fig. 6*G*); consistently, very little IκBα is found in the mitochondrial extracts of p62-KO HepG2 cells relative to those of corresponding p62-WT cells, both under basal conditions and upon IL-1β stimulation (Fig. 8*C*). And although, MG-132 rescues some of this nuclear IκBα content, it is still appreciably lower than that found in corresponding IL-1β–treated p62-WT cells. Furthermore, our findings of enhanced association of mitochondrial 28S ribosomal complex proteins with IκBα in the presence of p62-coexpression relative to its absence also support such a p62-assisted mitochondrial IκBα-import (Fig. 6*G*) Given that p62 is documented to promote proliferation and reduce apoptosis (58, 59) and mitochondrial IκBα is thought to serve a unique protective role against apoptosis, it is conceivable that by enhancing IκBα-mitochondrial import, p62 may similarly play a beneficial role in hepatic inflammatory responses.

Collectively, our findings document that p62 interacts with IκBα through a novel protein-interaction region which is independent of its many previously characterized structural protein-interacting regions including that with the innate defense regulator (IDR-1) peptide (38–45, 60). This p62–IκBα interaction region, however, not only comprises its NLS1 (42) but is also precisely the region known to interact with the mutant Cu-Zn superoxide dismutase, SOD1, a mutant linked to amyotrophic lateral sclerosis (61). The abrogation of such p62–IκBα interactions upon structural deletion of p62 PB1 domain suggested that such interactions could additionally require p62 oligomerization, as in the case of SOD1 (61). However, the following observations led us to exclude p62 oligomerization as a requirement for its IκBα interaction and stabilization: First, when the p62 K7A/D69A mutant that cannot self-oligomerize (62, 63) was examined, it failed to affect either IκBα interaction or its stabilization (*Preliminary Findings*). Second, should a p62 oligomer be required for recruiting IκBα, the chemical crosslinking analyses would document a majority of oligomers or at least trimers with two copies of p62 to one copy of IκBα. But the results of both the molecular mass upon SDS-PAGE analyses and the peptide count from the crosslinked species (generated intracellularly, prior to any potential oligomeric SDS-elicited disruption) reveal primarily a 1:1 stoichiometric ratio for p62 and IκBα. This combined evidence suggested that although p62 oligomerization is not essential for IκBα recruitment, the p62 PB1 domain is definitely important for its IκBα interaction. Intriguingly, in $p62^{f/f,Alb\text{-}Cre}$ mouse hepatocytes carrying the p62mut protein, in spite of its truncated PB-1 domain and its missing its OPCA motif (*acidic patch D69/D71/D73/E82*) that forms strong stabilizing salt bridges with R21–22 required for p62 dimerization, the p62mut protein is apparently capable of recruiting LC3 and forming autophagic puncta (supplemental Fig. S9), inferring that it is capable of oligomerization. Careful inspection of the p62mut sequence structure reveals that p62 contains another acidic patch E254/D256/D258/E260, which would become adjacent to R68 upon deletion of its 69 to 251 region. Thus, in this p62Δ 69 to 251 mutant, this juxtaposed region would now become E71/D73/D75/E77, which could very likely replace the deleted OPCA motif in the PB1 domain to form a stabilizing salt bridge with R21–22, thus retaining its ability to form oligomers.

Importantly, our documented IκBα–p62 interactions are critical not only for extending the cellular survival of IκBα (particularly, its readily degradable "free" *de novo*–synthesized species), but also in the absence of any canonical IκBα-NLS, p62 most likely enables its nuclear translocation, in addition to possibly also mediating its mitochondrial import. In HepG2-cells, p62-KO not only enhanced TNFα- or IL-1β–elicited nuclear NF-κB-activation but also prolonged its nuclear persistence. Furthermore, we found that mouse hepatocytes genetically deficient in this IκBα-interacting p62 subdomain also exhibit prolonged IL-1β–elicited NF-κB activation. More importantly, our findings that progressively severe hepatic inflammation is observed with aging in intact mice with a genetic deficiency in this hepatic IκBα-interacting p62 subdomain (Fig. 9*C* and supplemental Fig. S10) reveal that such an IκBα–p62 interaction is physiologically and pathophysiologically relevant. The p62 protein scaffold is known to modulate NF-κB activation both positively and negatively through direct and/or indirect interactions with various cell-specific interactors and/or signaling effectors at one of its many defined structural subdomains (15, 64). Our findings detailed above further expand this growing repertoire of p62-elicited NF-κB modulation by revealing a novel, albeit fundamental mode of p62-mediated regulation of NF-κB activation through its interplay with IκBα. Furthermore, they provide a belated rationale for the then "puzzling" report that in contrast to other scenarios, p62 accumulation in autophagy-deficient immortalized baby mouse kidney cells led to the inhibition of the canonical NF-κB activation pathway (64, 65).

DATA AVAILABILITY

RAW mass spectrometry data are deposited in the MassIVE repository (https://massive.ucsd.edu) with accession number: MSV000090324. (*reviewer password: ikba2022*).

Annotated peak lists supporting the crosslinked spectral assignments are available on MS-Viewer (https://msviewer.ucsf.edu/cgi-bin/msform.cgi?form=msviewer).

Search key (DSS crosslinks): MS-Viewer, ex4ngmrtrj

Search key (SIAB crosslinks): MS-Viewer, l2srapmex0

Supplemental data—This article contains supplemental data.

Acknowledgments—We gratefully acknowledge Mr Chris Her, UCSF Liver Cell & Tissue Biology Core Facility for hepatocyte isolation and the UCSF Liver Center Pathology Core for the histopathological analyses, both supported by NIDDK Grant P30DK26743. We also sincerely thank Prof. Haining Zhu, University of Kentucky, for providing p62-KO MEF cells generated in Prof. M. Komatsu's lab, Niigata University, Japan. An UCSF Liver Center Flex fund (NIDDK Grant P30DK26743) supported the generation of the genetic p62mut mouse through UC Davis KOMP Facility. We also acknowledge the support for the mass spectrometry experiments at the UCSF Biomedical Mass Spectrometry and Proteomics Resource Center (Prof. A. L. Burlingame, Director) by the Adelson Medical Research Foundation and the University of California, San Francisco Program for Breakthrough Biomedical Research.

Funding and additional information—These studies were supported by NIH Grants GM44037 (M. A. C.). The content is solely the responsibility of the authors and does not necessarily represent the official views of the National Institutes of Health.

Author contributions—Y. L., M. J. T., M. A. C., and A. L. B. methodology; Y. L., M. J. T., and M. A. C. writing–original draft; M. A. C. and A. L. B. supervision; Y. L. investigation; Y. L. and L. H. formal analysis; Y. L. data curation; Y. L., M. J. T., L. H., A. L. B., and M. A. C. writing–review and editing.

Conflict of interest—The authors declare that they have no conflicts of interest with the contents of this article.

Abbreviations—The abbreviations used are: ABC, ammonium bicarbonate; AGC, automatic gain control; AR, Ankyrin repeat; ARD, AR-domain; CE, cytoplasmic extract; Co-IP, co-immunoprecipitation; DSS, disuccinimidyl suberate; FBS, fetal bovine serum; FDR, false discovery rates; HA, hemagglutinin; HA-IκBα, HA-tagged IκBα; HCD, higher-energy collisional dissociation; IB, Immunoblotting; IDR-1, innate defense regulator; IL-1β, interleukin-1β; IκB, NF-κB inhibitor; IR, intervening region; Lys-C, lysylendopeptidase C; MEFs, mouse embryo fibroblasts; NCE, normalized collision energy; NF-κB, nuclear factor kappa-light-chain-enhancer of activated B cells; NIS, nuclear import sequences; NLS, nuclear localization signal; NSAF, normalized spectral abundance factor; Nup153, nucleoporin 153; p62 flp/flp, p62-floxed mouse; p62-Myc, Myc-tagged p62; p62mut, p62 genetic mutant mouse; PB-1, Phox and Bem1p-domain; P-p65, phosphorylated p65; RanBP2, a SUMO E3-ligase/Nup358; Ran-GDP, an abundant GTPase involved in nuclear import; SA, streptavidin; SIAB, (succinimidyl (4-iodoacetyl)aminobenzoate); SOD1, Cu-Zn superoxide dismutase; SQSTM-1, Sequestosome 1; TB, TRAF6-binding; TNFα, tumor necrosis factor α; Ub, ubiquitin; XLMS, chemical crosslinking mass spectrometry; ZnPP, Zn-protoporphyrin IX; ZZ, Zn-finger binding motifs.

Received October 14, 2022, and in revised form, January 2, 2023
Published, MCPRO Papers in Press, January 10, 2023, https://doi.org/10.1016/j.mcpro.2023.100495

REFERENCES

1. Liou, H. C., and Baltimore, D. (1993) Regulation of the NF-kappa B/rel transcription factor and I kappa B inhibitor system. *Curr. Opin. Cell Biol.* **5**, 477–487
2. Azimifar, S. B., Nagaraj, N., Cox, J., and Mann, M. (2014) Cell-type-resolved quantitative proteomics of murine liver. *Cell Metab.* **20**, 1076–1087
3. Han, Y., and Brasier, A. R. (1997) Mechanism for biphasic rel A. NF-kappaB1 nuclear translocation in tumor necrosis factor alpha-stimulated hepatocytes. *J. Biol. Chem.* **272**, 9825–9832
4. Rao, P., Hayden, M. S., Long, M., Scott, M. L., West, A. P., Zhang, D., *et al*. (2010) IkappaBbeta acts to inhibit and activate gene expression during the inflammatory response. *Nature* **466**, 1115–1119
5. Wisniewski, J. R., Vildhede, A., Noren, A., and Artursson, P. (2016) In-depth quantitative analysis and comparison of the human hepatocyte and hepatoma cell line HepG2 proteomes. *J. Proteomics* **136**, 234–247
6. Beg, A. A., Finco, T. S., Nantermet, P. V., and Baldwin, A. S., Jr. (1993) Tumor necrosis factor and interleukin-1 lead to phosphorylation and loss of I kappa B alpha: a mechanism for NF-kappa B activation. *Mol. Cell. Biol.* **13**, 3301–3310
7. Traenckner, E. B., Wilk, S., and Baeuerle, P. A. (1994) A proteasome inhibitor prevent activation of NF-kappa B and stabilizes a newly phosphorylated form of I kappa B-alpha that is still bound to NF-kappa B. *EMBO J.* **13**, 5433–5441
8. Weil, R., Laurent-Winter, C., and Israël, A. (1997) Regulation of IkappaBbeta degradation. Similarities to and differences from IkappaBalpha. *J. Biol. Chem.* **272**, 9942–9949
9. Arenzana-Seisdedos, F., Thompson, J., Rodriguez, M. S., Bachelerie, F., Thomas, D., and Hay, R. T. (1995) Inducible nuclear expression of newly synthesized I kappa B alpha negatively regulates DNA-binding and transcriptional activities of NF-kappa B. *Mol. Cell. Biol.* **15**, 2689–2696
10. Thompson, J. E., Phillips, R. J., Erdjument-Bromage, H., Tempst, P., and Ghosh, S. (1995) I kappa B-beta regulates the persistent response in a biphasic activation of NF-kappa B. *Cell* **80**, 573–582
11. Arenzana-Seisdedos, F., Turpin, P., Rodriguez, M., Thomas, D., Hay, R. T., Virelizier, J. L., *et al*. (1997) Nuclear localization of I kappa B alpha promotes active transport of NF-kappa B from the nucleus to the cytoplasm. *J. Cell Sci.* **110**, 369–378
12. Ghosh, S., and Karin, M. (2002) Missing pieces in the NF-kappaB puzzle. *Cell* **109 Suppl**, S81–S96
13. Vadlamudi, R. K., and Shin, J. (1998) Genomic structure and promoter analysis of the p62 gene encoding a non-proteasomal multiubiquitin chain binding protein. *FEBS Lett.* **435**, 138–142
14. Chen, C., Deng, M., Sun, Q., Loughran, P., Billiar, T. R., and Scott, M. J. (2014) Lipopolysaccharide stimulates p62-dependent autophagy-like aggregate clearance in hepatocytes. *Biomed. Res. Int.* **2014**, 267350
15. Manley, S., Williams, J. A., and Ding, W. X. (2013) Role of p62/SQSTM1 in liver physiology and pathogenesis. *Exp. Biol. Med. (Maywood)* **238**, 525–538
16. Zhong, Z., Sanchez-Lopez, E., and Karin, M. (2016) Autophagy, inflammation, and immunity: a Troika governing cancer and its treatment. *Cell* **166**, 288–298
17. Ling, J., Kang, Y., Zhao, R., Xia, Q., Lee, D. F., Chang, Z., *et al*. (2012) KrasG12D-induced IKK2/beta/NF-kappaB activation by IL-1alpha and

p62 feedforward loops is required for development of pancreatic ductal adenocarcinoma. *Cancer Cell* **21**, 105–120
18. Taniguchi, K., Yamachika, S., He, F., and Karin, M. (2016) p62/SQSTM1-Dr. Jekyll and Mr. Hyde that prevents oxidative stress but promotes liver cancer. *FEBS Lett.* **590**, 2375–2397
19. Dembinski, H. E., Wismer, K., Vargas, J. D., Suryawanshi, G. W., Kern, N., Kroon, G., *et al*. (2017) Functional importance of stripping in NFκB signaling revealed by a stripping-impaired IκBα mutant. *Proc. Natl. Acad. Sci. U. S. A.* **114**, 1916–1921
20. O'Dea, E. L., Barken, D., Peralta, R. Q., Tran, K. T., Werner, S. L., Kearns, J. D., *et al*. (2007) A homeostatic model of IkappaB metabolism to control constitutive NF-kappaB activity. *Mol. Syst. Biol.* **3**, 111
21. Liu, Y., Trnka, M. J., Guan, S., Kwon, D., Kim, D. H., Chen, J. J., *et al*. (2020) A novel mechanism for NF-kappaB-activation via IkappaB-aggregation: implications for hepatic Mallory-Denk-body induced inflammation. *Mol. Cell. Proteomics* **19**, 1968–1986
22. Komatsu, M., Waguri, S., Koike, M., Sou, Y. S., Ueno, T., Hara, T., *et al*. (2007) Homeostatic levels of p62 control cytoplasmic inclusion body formation in autophagy-deficient mice. *Cell* **131**, 1149–1163
23. Hsu, P. D., Scott, D. A., Weinstein, J. A., Ran, F. A., Konermann, S., Agarwala, V., *et al*. (2013) DNA targeting specificity of RNA-guided Cas9 nucleases. *Nat. Biotechnol.* **31**, 827–832
24. Han, X. M., Lee, G., Hefner, C., Maher, J. J., and Correia, M. A. (2005) Heme-reversible impairment of CYP2B1/2 induction in heme-depleted rat hepatocytes in primary culture: translational control by a hepatic alpha-subunit of the eukaryotic initiation factor kinase? *J. Pharmacol. Exp. Ther.* **314**, 128–138
25. Ran, F. A., Hsu, P. D., Wright, J., Agarwala, V., Scott, D. A., and Zhang, F. (2013) Genome engineering using the CRISPR-Cas9 system. *Nat. Protoc.* **8**, 2281–2308
26. Hung, V., Lam, S. S., Udeshi, N. D., Svinkina, T., Guzman, G., Mootha, V. K., *et al*. (2017) Proteomic mapping of cytosol-facing outer mitochondrial and ER membranes in living human cells by proximity biotinylation. *Elife* **6**, e24463
27. Rosenfeld, J., Capdevielle, J., Guillemot, J. C., and Ferrara, P. (1992) In-gel digestion of proteins for internal sequence analysis after one- or two-dimensional gel electrophoresis. *Anal. Biochem.* **203**, 173–179
28. Hellman, U., Wernstedt, C., Gonez, J., and Heldin, C. H. (1995) Improvement of an "in-gel" digestion procedure for the micropreparation of internal protein fragments for amino acid sequencing. *Anal. Biochem.* **224**, 451–455
29. Chalkley, R. J., Baker, P. R., Medzihradszky, K. F., Lynn, A. J., and Burlingame, A. L. (2008) In-depth analysis of tandem mass spectrometry data from disparate instrument types. *Mol. Cell. Proteomics* **7**, 2386–2398
30. Elias, J. E., and Gygi, S. P. (2007) Target-decoy search strategy for increased confidence in large-scale protein identifications by mass spectrometry. *Nat. Methods* **4**, 207–214
31. Zybailov, B., Mosley, A. L., Sardiu, M. E., Coleman, M. K., Florens, L., and Washburn, M. P. (2006) Statistical analysis of membrane proteome expression changes in Saccharomyces cerevisiae. *J. Proteome Res.* **5**, 2339–2347
32. Teo, G., Liu, G., Zhang, J., Nesvizhskii, A. I., Gingras, A. C., and Choi, H. (2014) SAINTexpress: improvements and additional features in significance analysis of INTeractome software. *J. Proteomics* **100**, 37–43
33. Mellacheruvu, D., Wright, Z., Couzens, A. L., Lambert, J. P., St-Denis, N. A., Li, T., *et al*. (2013) The CRAPome: a contaminant repository for affinity purification-mass spectrometry data. *Nat. Methods* **10**, 730–736
34. Cox, J., and Mann, M. (2008) MaxQuant enables high peptide identification rates, individualized p.p.b.-range mass accuracies and proteome-wide protein quantification. *Nat. Biotechnol.* **26**, 1367–1372
35. Mathes, E., O'Dea, E. L., Hoffmann, A., and Ghosh, G. (2008) NF-kappaB dictates the degradation pathway of IkappaBalpha. *EMBO J.* **27**, 1357–1367
36. Fortmann, K. T., Lewis, R. D., Ngo, K. A., Fagerlund, R., and Hoffmann, A. (2015) A regulated, ubiquitin-independent degron in IkappaBalpha. *J. Mol. Biol.* **427**, 2748–2756
37. Miyamoto, S., Maki, M., Schmitt, M. J., Hatanaka, M., and Verma, I. M. (1994) Tumor necrosis factor alpha-induced phosphorylation of I kappa B alpha is a signal for its degradation but not dissociation from NF-kappa B. *Proc. Natl. Acad. Sci. U. S. A.* **91**, 12740–12744
38. Pankiv, S., Clausen, T. H., Lamark, T., Brech, A., Bruun, J. A., Outzen, H., *et al*. (2007) p62/SQSTM1 binds directly to Atg8/LC3 to facilitate degradation of ubiquitinated protein aggregates by autophagy. *J. Biol. Chem.* **282**, 24131–24145
39. Moscat, J., Diaz-Meco, M. T., and Wooten, M. W. (2007) Signal integration and diversification through the p62 scaffold protein. *Trends Biochem. Sci.* **32**, 95–100
40. Ichimura, Y., Kumanomidou, T., Sou, Y. S., Mizushima, T., Ezaki, J., Ueno, T., *et al*. (2008) Structural basis for sorting mechanism of p62 in selective autophagy. *J. Biol. Chem.* **283**, 22847–22857
41. Komatsu, M., and Ichimura, Y. (2010) Physiological significance of selective degradation of p62 by autophagy. *FEBS Lett.* **584**, 1374–1378
42. Pankiv, S., Lamark, T., Bruun, J. A., Overvatn, A., Bjorkoy, G., and Johansen, T. (2010) Nucleocytoplasmic shuttling of p62/SQSTM1 and its role in recruitment of nuclear polyubiquitinated proteins to promyelocytic leukemia bodies. *J. Biol. Chem.* **285**, 5941–5953
43. Lin, X., Li, S., Zhao, Y., Ma, X., Zhang, K., He, X., *et al*. (2013) Interaction domains of p62: a bridge between p62 and selective autophagy. *DNA Cell Biol.* **32**, 220–227
44. Somlapura, M., Gottschalk, B., Lahiri, P., Kufferath, I., Pabst, D., Rulicke, T., *et al*. (2021) Different roles of p62 (SQSTM1) isoforms in keratin-related protein aggregation. *Int. J. Mol. Sci.* **22**, 6227
45. Jacobs, M. D., and Harrison, S. C. (1998) Structure of an IkappaBalpha/NF-kappaB complex. *Cell* **95**, 749–758
46. Jaffray, E., Wood, K. M., and Hay, R. T. (1995) Domain organization of I kappa B alpha and sites of interaction with NF-kappa B p65. *Mol. Cell. Biol.* **15**, 2166–2172
47. Bergqvist, S., Ghosh, G., and Komives, E. A. (2008) The IkappaBalpha/NF-kappaB complex has two hot spots, one at either end of the interface. *Protein Sci.* **17**, 2051–2058
48. Zabel, U., Henkel, T., Silva, M. S., and Baeuerle, P. A. (1993) Nuclear uptake control of NF-kappa B by MAD-3, an I kappa B protein present in the nucleus. *EMBO J.* **12**, 201–211
49. Sachdev, S., Hoffmann, A., and Hannink, M. (1998) Nuclear localization of IkappaB alpha is mediated by the second ankyrin repeat: the IkappaB alpha ankyrin repeats define a novel class of cis-acting nuclear import sequences. *Mol. Cell. Biol.* **18**, 2524–2534
50. Turpin, P., Hay, R. T., and Dargemont, C. (1999) Characterization of IkappaBalpha nuclear import pathway. *J. Biol. Chem.* **274**, 6804–6812
51. Lu, M., Zak, J., Chen, S., Sanchez-Pulido, L., Severson, D. T., Endicott, J., *et al*. (2014) A code for RanGDP binding in ankyrin repeats defines a nuclear import pathway. *Cell* **157**, 1130–1145
52. Bayliss, R., Ribbeck, K., Akin, D., Kent, H. M., Feldherr, C. M., Gorlich, D., *et al*. (1999) Interaction between NTF2 and xFxFG-containing nucleoporins is required to mediate nuclear import of RanGDP. *J. Mol. Biol.* **293**, 579–593
53. Nakielny, S., Shaikh, S., Burke, B., and Dreyfuss, G. (1999) Nup153 is an M9-containing mobile nucleoporin with a novel Ran-binding domain. *EMBO J.* **18**, 1982–1995
54. Partridge, J. R., and Schwartz, T. U. (2009) Crystallographic and biochemical analysis of the Ran-binding zinc finger domain. *J. Mol. Biol.* **391**, 375–389
55. Hamada, M., Haeger, A., Jeganathan, K. B., van Ree, J. H., Malureanu, L., Walde, S., *et al*. (2011) Ran-dependent docking of importin-beta to RanBP2/Nup358 filaments is essential for protein import and cell viability. *J. Cell Biol.* **194**, 597–612
56. Walde, S., Thakar, K., Hutten, S., Spillner, C., Nath, A., Rothbauer, U., *et al*. (2012) The nucleoporin Nup358/RanBP2 promotes nuclear import in a cargo- and transport receptor-specific manner. *Traffic* **13**, 218–233
57. Zhong, Z., Umemura, A., Sanchez-Lopez, E., Liang, S., Shalapour, S., Wong, J., *et al*. (2016) NF-kappaB restricts inflammasome activation via elimination of damaged mitochondria. *Cell* **164**, 896–910
58. Duran, A., Linares, J. F., Galvez, A. S., Wikenheiser, K., Flores, J. M., Diaz-Meco, M. T., *et al*. (2008) The signaling adaptor p62 is an important NF-kappaB mediator in tumorigenesis. *Cancer Cell* **13**, 343–354
59. Moscat, J., Karin, M., and Diaz-Meco, M. T. (2016) p62 in cancer: signaling adaptor beyond autophagy. *Cell* **167**, 606–609
60. Yu, H. B., Kielczewska, A., Rozek, A., Takenaka, S., Li, Y., Thorson, L., *et al*. (2009) Sequestosome-1/p62 is the key intracellular target

of innate defense regulator peptide. *J. Biol. Chem.* **284**, 36007–36011
61. Gal, J., Strom, A. L., Kwinter, D. M., Kilty, R., Zhang, J., Shi, P., *et al*. (2009) Sequestosome 1/p62 links familial ALS mutant SOD1 to LC3 via an ubiquitin-independent mechanism. *J. Neurochem.* **111**, 1062–1073
62. Lamark, T., Perander, M., Outzen, H., Kristiansen, K., Overvatn, A., Michaelsen, E., *et al*. (2003) Interaction codes within the family of mammalian Phox and Bem1p domain-containing proteins. *J. Biol. Chem.* **278**, 34568–34581
63. Hirano, Y., Yoshinaga, S., Ogura, K., Yokochi, M., Noda, Y., Sumimoto, H., *et al*. (2004) Solution structure of atypical protein kinase C PB1 domain and its mode of interaction with ZIP/p62 and MEK5. *J. Biol. Chem.* **279**, 31883–31890
64. Moscat, J., and Diaz-Meco, M. T. (2009) p62 at the crossroads of autophagy, apoptosis, and cancer. *Cell* **137**, 1001–1004
65. Mathew, R., Karp, C. M., Beaudoin, B., Vuong, N., Chen, G., Chen, H. Y., *et al*. (2009) Autophagy suppresses tumorigenesis through elimination of p62. *Cell* **137**, 1062–1107